Adaptive Multi-UAV Relay Deployment Framework in Satellite Aerial Ground Integrated Systems

Bhola, *Member, IEEE*, Yu-Jia Chen, *Senior Member, IEEE*, Ashutosh Balakrishnan, *Member, IEEE*, Swades De, *Senior Member, IEEE*, and Li-Chun Wang, *Fellow, IEEE*

***Abstract*—The sixth-generation (6G) communication networks are expected to provide high data rates, ultra-reliable communication, and massive connectivity, especially in challenging environments such as dense urban areas and disaster-affected regions. However, traditional terrestrial-only networks face significant challenges in these scenarios, including signal blockages from high-rise buildings, traffic congestion, and dynamic user distributions. To address these limitations, we propose the adaptive multi-UAV deployment (AMUD) framework within satellite air-ground integrated networks (SAGINs). The AMUD framework dynamically deploys amplify-and-forward multiple unmanned aerial vehicle relay (UAVr) in with low Earth orbit (LEO) satellites to improve coverage, alleviate congestion, and ensure reliable communication in non-line-of-sight and high-demand conditions. We formulate an optimization problem that aims to jointly maximize the energy efficiency of the total network and the total capacity while ensuring the fairness of the total capacity and satisfying the user's requirements. The simulation results demonstrate that AMUD improves the total capacity of the network, improves the total energy efficiency, and increases the fairness of the capacity compared to traditional LEO satellite and ground base station (LEO-GBS) only systems.**

***Index Terms*—6G Networks, LEO satellites, multiple UAVr, SAGIN, cooperative diversity, demand-supply aware balance.**

TABLE I: Key Notations

Symbol	Definition
$\mathbf{u}_i$	2D location vector of user i at time t
$\mathbf{U}_j$	3D location vector of UAVr j at time t
$\mathbf{h}_{i\leftarrow s}$	Channel vector from the satellite to user i (L antennas)
$\hbar_{j\leftarrow s}$	Scalar channel coefficient from the satellite to UAVr j
$\mathbf{h}_{i\leftarrow j}$	Channel vector from UAVr j to user i (L antennas)
x_{sym}	Symbol transmitted by the satellite
P_s^{tx}	Satellite transmit power
$p_{i\leftarrow j}$	Transmit power from UAVr j to user i
$\mathcal{G}$	Amplify-and-forward gain at the UAVr
$\mathbf{n}_{i\leftarrow s}$	AWGN vector at user i from the satellite link
$n_{j\leftarrow s}$	Scalar AWGN at UAVr j from the satellite
$\mathbf{r}^{i\leftarrow s}$	Received signal vector at user i from the satellite
$r^{j\leftarrow s}$	Received signal at UAVr j from the satellite
$\mathbf{r}^{i\leftarrow j\leftarrow s}$	Received signal vector at user i after relay forwarding
$\gamma_{i\leftarrow j}$	SINR of the UAVr-to-user link
$\gamma_{j\leftarrow s}$	SINR of the satellite-to-UAVr link
$\gamma_{i\leftarrow s}$	SINR of the satellite-to-user link
$V_{j\leftarrow s}$	Satellite visibility indicator for UAVr j
p_j^{Hov}	Hovering power consumption of UAVr j
C_j	Data rate of the UAVr-assisted link
C_G	Data rate of the GBS link
C_{Tot}	Total system network capacity
p_j^{Total}	Total power consumption of UAVr j
E_{Tot}	System energy efficiency

I. Introduction

THE demand for reliable wireless access has grown significantly, driven by emerging technologies such as augmented reality, the Internet of Things (IoT), and autonomous vehicles. By 2023, Cisco projects that mobile users will reach 13.1 billion globally, with 29.3 billion devices enabled by the Internet [2]. This surge in demand and increasing quality of service (QoS) requirements lead to dynamic user traffic and hotspots that vary in space-time within wireless networks [3]. Although ground base stations (GBS) have traditionally served network users, they struggle with increasing user density and signal blockages, especially in urban environments. These random non-line-of-sight (NLOS) conditions and obstructions degrade service quality, creating the need for more agile network solutions.

To address these limitations, 6G communication networks are expected to integrate terrestrial and non-terrestrial elements (i.e., aerial and space-based technologies) to enhance network capacity and resilience [1], [4], [5]. Satellite air-ground integrated networks (SAGINs) are considered a key enabler of scalable, dynamic, and adaptive 6G systems [6]. This paper introduces an AMUD framework within SAGINs that dynamically deploys unmanned aerial vehicle relay (UAVr) to improve coverage and signal-to-interference-plus-noise ratio (SINR), especially for users facing signal blockages or GBS congestion. The framework aligns with the 6G vision by addressing urban communication bottlenecks and enabling flexible, aerial-ground cooperative relay strategies.

A. Motivation

Recent interest has focused on integrating terrestrial networks with space-based LEO satellites to provide seamless connectivity and high-speed broadband access for 6G communications. LEO satellite networks consist of a mega-constellation of satellites and wireless backbones. Traditionally, satellites have been used primarily for communication in rural areas. However, in urban environments, satellite links are susceptible

An early version of this work was presented at the IEEE Vehicular Technology Conference (VTC-Fall) 2024 [1].

Bhola is with the Department of Electrical and Computer Engineering, National Yang Ming Chiao Tung University, Taiwan R.O.C. (email: bhola.ee06@nycu.edu.tw)

Yu-Jia Chen is with the National Central University, Chung-Li 32001, Taiwan (e-mail: yjchen@ce.ncu.edu.tw)

A. Balakrishnan is with the Department of Computer Science and Networks, Télécom Paris, 91120 Paris, France. (email: balakrishnan@telecom-paris.fr)

S. De is with the Department of Electrical Engineering and Bharti School of Telecommunication, Indian Institute of Technology Delhi, New Delhi, India. (email: swadesd@ee.iitd.ac.in)

L.-C. Wang is with the Department of Electrical and Computer Engineering, National Yang Ming Chiao Tung University, Taiwan R.O.C. (email:wang@nycu.edu.tw) *(Corresponding author: Li-Chun Wang.)*

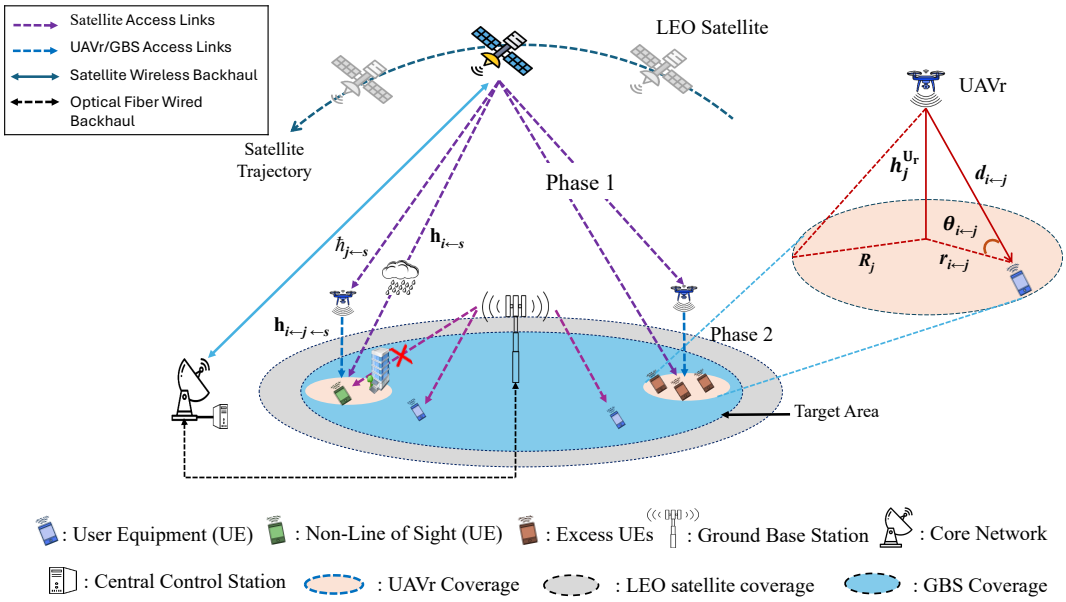

Fig. 1: System Model: Hybrid Network Overview.

to masking effects caused by climatic conditions (e.g., rain, fog) and terrestrial obstructions (e.g., tunnels, dense buildings), which significantly attenuate signals reaching ground users [7]. Furthermore, satellite links, especially those that involve LEO satellites, face challenges in adapting to dynamic network conditions due to their inherent mobility and rapid temporal variations in Internet usage patterns [8]. Although LEO satellites experience lower latency compared to medium-earth orbit (MEO) and geostationary earth orbit (GEO) satellites, their shorter orbital paths require continuous tracking of satellite movement related to the ground area under observation [9]–[12]

Despite these urban propagation challenges, LEO satellites are increasingly being considered for urban coverage to support seamless global access, offload congested terrestrial networks, and maintain service continuity during infrastructure outages or disasters. However, their practical utility in urban environments is critically dependent on solving the limitations of NLoS imposed by urban obstructions. To this end, UAVr serve as agile intermediaries that can dynamically bridge the NLoS gap between satellites and users, ensuring robust and adaptive urban connectivity. The deployment of unmanned aerial vehicles as base stations (UAV-BS) has been a conventional method to increase capacity in terrestrial networks [13]–[17]. In this paper, we propose the deployment of low-altitude UAVr to address the challenges associated with integrating LEO satellites and improving user QoS. The proposed strategy of deploying multiple UAVr is more energy efficient than traditional UAV-BS while effectively meeting user QoS requirements. Additionally, unlike terrestrial relays in heterogeneous networks, multiple UAVr offer mobility to the mobile operator. This capability allows multiple UAVr to be deployed in rural or disaster scenarios, such as floods, where traditional infrastructure may be compromised.

This paper proposes an adaptive multi-UAVr deployment framework (AMUD) for air-ground satellite integrated networks. In a fixed terrestrial area under observation, particularly with space-time-varying traffic hotspots, the AMUD framework first computes optimal locations for deploying multiple UAVr based on traffic demand distribution. The framework improves network capacity and energy efficiency by improving user QoS. User QoS is improved by exploiting spatial diversity through a cooperative diversity (CD) strategy at the ground user level, which combines signals from separate communication links from LEO satellites and multiple UAVr. The AMUD framework intelligently controls multiple UAVr and signals to provide fair communication opportunities to users within the designated experimental terrestrial coverage area. The key contributions of this work are summarized as follows:

- This study presents an innovative architecture that establishes a multilayered communication network that seamlessly integrates multiple UAVr, LEO satellites, and GBS. This configuration enables flexible and dynamic coverage, effectively addressing congestion challenges and enhancing network adaptability. The deployment of multiple UAVr provides localized coverage in regions with varying user densities, while LEO satellites offer extensive coverage and high data transmission rates. The architecture explicitly incorporates satellite visibility and fairness considerations to ensure reliable communication in both urban and remote environments.
- We propose the AMUD framework, a pioneering approach that combines cooperative UAVr with the LEO satellite to overcome NLoS challenges in densely populated urban settings. The framework employs amplify and forward techniques with cooperative diversity combining, allowing weighted SINR fusion of satellite–user and UAVr–user links to improve signal quality and network robustness. This dynamic approach addresses coverage gaps and congestion issues, significantly improving network capacity and energy efficiency compared to conventional systems

lacking fairness or visibility awareness.
- An optimization problem is formulated to maximize the network's total energy efficiency and capacity while ensuring fairness among ground users. The proposed framework optimizes user association and transmission power allocation strategies unifying these objectives within a single formulation. This integrated optimization ensures efficient resource utilization and improved performance in SAGINs.

B. Organization

Section II presents and positions the work in the current literature. Section III presents the system model, while Section IV details the proposed AMUD framework. Section V formulates a network energy efficiency maximization problem, and Section VI presents an algorithmic solution framework. Section VII shows the simulation and performance analysis results, while Section VIII concludes the paper.

II. Related Work

This section reviews recent literature on enhancing the network capacity in SAGINs and positions the contribution of the paper. Table II summarizes the related work and positions the proposed AMUD framework in terms of the type of relay, number of relays used, adaptive deployment of UAVr, access link, satellite visibility, and signal combination strategy employed. Several recent studies have presented deployment methods to enhance network performance, considering static and mobile relay deployment without accounting for satellite visibility and adaptive relay deployment.

Recent studies have concentrated on the deployment of static terrestrial relays to enhance network performance in designated regions by integrating these relays with satellite access links [12], [18]–[21]. In [18], the authors examined the ergodic capacity of hybrid satellite-terrestrial networks (HSTNs) that incorporate multiple terrestrial relays in addition to a direct satellite link. They utilized asymptotic analysis for both AF and decode-and-forward (DF) protocols, employing moment-generating function (MGF) techniques. A relay selection strategy was proposed based on statistical information from channel state information (CSI) to reduce overhead. The framework presented in [20] employs a cooperative approach that integrates direct and terrestrial relay links to enhance diversity. Huang et al. [19] formulated an optimization problem aimed at maximizing the system's capacity within HSTNs subject to shadowed Rician fading, deriving expressions for outage probability and ergodic capacity while introducing strategies for multi-user scheduling. Zhao et al. [12] investigated the ergodic capacity of a generalized HSTN featuring multiple relays and a direct satellite link. They applied MGF techniques for the AF and DF protocols and proposed a relay selection strategy that minimizes reliance on statistical CSI. Finally, the work in [21] explores the synergy between satellite and terrestrial relays within a dual-hop system, focusing on ergodic capacity and bit error rate under varying channel conditions. An opportunistic relay approach was used to support multiple users effectively. Recent studies have concentrated on strategies for the deployment of UAVs to improve network performance by using satellite access [7], [22]–[27]. In [7], machine learning techniques were used to address link selection and UAV trajectory challenges within UAV-assisted hybrid satellite-terrestrial networks. Although notable improvements were achieved, the strategic placement of UAVs to alleviate congestion in satellite backhaul remains an open issue. Furthermore, incorporating cyclical patterns into UAV trajectory planning could optimize resource utilization and improve overall network efficiency. The research presented in [25] investigated multi-user asymmetric free-space optical (FSO) and radio frequency (RF) links between satellites and UAVs, accounting for Gamma-Gamma turbulence effects. The findings revealed a trade-off between fairness and system capacity when UAV trajectories were fixed. In the realm of relay systems enabled by ultra-reliable low-latency communication (URLLC) assisted by UAVs, [26] used the Nelder-Mead simplex search algorithm to optimize the height and positioning of UAVs in conjunction with the allocation of block length. This approach aimed to minimize decoding errors while maintaining fixed UAV paths in conjunction with reconfigurable intelligent surfaces (RIS). Finally, [27] introduced a Gibbs sampling method for optimal placement of UAVs as relay nodes, focusing on maximizing the minimum achievable rate for multiple pairs of ground nodes while keeping the UAV trajectories constant.

To improve user QoS at the receiver end, recent research efforts (e.g. [28], [29]) have proposed integrated techniques aimed at improving network performance, particularly through cooperative communication schemes. The study in [28] evaluates the effectiveness of cooperative communication using receiver-end selection combining (SC) on a Nakagami fading channel. In [29], a novel cooperative space-shift keying network is introduced, featuring multi-antenna configurations for the source, destination, and relays. This approach involves selecting relays based on predetermined thresholds during the second time slot for data transmission from the source to the destination, where successive interference cancelation is employed for detection. The authors performed a comprehensive theoretical analysis of error performance, specifically addressing the scenario with two transmit antennas at the source and providing an analytical approximation for more general cases.

As shown in Table II, existing work has focused on optimizing traffic offloading to maximize user service and system capacity. These works primarily focus on single or multiple UAV-BS deployments with or without satellite access. Recent studies have yet to comprehensively address the effects of adaptive multiple UAVr deployment, satellite visibility, and signal-combining techniques. Our proposed AMUD approach addresses all of these limitations. It jointly considers the adaptive deployment of multiple UAVr considering the visibility of the LEO satellite. The proposed framework also involves power control transmission on the UAVr and a combination of spacetime signals on the receiver using CD. We present the system model in the next section.

III. System Model

The paper considers downlink resource allocation in a terrestrial network assisted by multiple UAVr and LEO satellites,

TABLE II: Comparison of Representative Works on Relay-Based Access Architectures in SAGIN

Ref.	Relay Type	Relay Count	Trajectory Pattern	Adaptive UAVr	Satellite Consideration	Satellite Visibility	Capacity Fairness
[18], [19]	Static	Single Terrestrial	–	–	Yes	–	–
[12], [20]	Static	Multi Terrestrial	–	–	Yes	–	–
[21]	Static	Multi Terrestrial	–	–	Yes	–	–
[22]	Mobile	Single UAVr	–	–	Yes	–	–
[23], [24]	Mobile	Single UAVr	Cyclical	–	Yes	–	–
[25]	Mobile	Single UAVr	Fixed	–	Yes	–	Yes
[7]	Mobile	Multi UAVr	Cyclical	–	Yes	–	–
[26]	Mobile	Single UAVr	Fixed	–	–	–	–
[27]	Mobile	Multi UAVr	Fixed	–	–	–	–
Our Method	**Mobile**	**Multi UAVr**	**Fixed**	**Yes**	**Yes**	**Yes**	**Yes**

Note: This table focuses on relay-based architectures involving UAVr access link studies. As described in Section II, UAVr nodes do not serve as direct access points but instead relay traffic via the nearest GBS or satellite.

as illustrated in Fig. 1. The set of ground users is represented and modeled as a Poisson point process (PPP) within the GBS coverage area. In our simulation, urban hotspots are generated based on two criteria: (1) density-based, where the user density within a UAVr's coverage area exceeds a predefined threshold $\omega_j^{\max} = D_j^{\text{th}} \cdot \pi \cdot R_j^2$, and (2) user-based, where the number of users in a GBS area exceeds its capacity, forming excess users $\Omega_{\mathbb{G}}^{\text{Ex}} = \Omega_{\mathbb{G}} - \omega_{\mathbb{G}}^{\max}$. These dynamic conditions trigger UAV assistance for load balancing. We examine the dynamic behavior of the network on a set χ comprising $\varkappa$ time intervals indexed by t. The network configuration is considered stable given the brief duration of each time slot. We denote the two-dimensional coordinates of ground users in the time slot t as $\mathbf{u}_i(t) = (x_i(t), y_i(t))$, where $i \in \{1, \ldots, N\}$ and N indicate the total number of users in the system. The framework enables the deployment of up to K multiple UAVr, represented as $\mathbf{U}_j(t) = (x_j(t), y_j(t), h_j^{\text{Ur}}(t))$, where $j \in \{1, \ldots, K\}$, within the coverage area. "It is important to note that although the user locations are monitored in real time, the deployment of UAVr is based on the final snapshot sampled within each interval. Once deployed, UAVr positions remain fixed, and thus the system behaves equivalently to a static deployment." Let $p_{i \leftarrow j}$ denote the minimum transmit power required to send a signal from the UAVr to the ground user.

We ignore the effects of changes in the UAVr's three-dimensional (3D) position on the LEO satellite. The central control station (CCS) continuously monitors UAVr movement, determining user associations with multiple UAVr and preventing collisions between them. Mobile users are considered hybrid [30], capable of communicating with LEO satellites, multiple UAVr, and GBS. Users communicate with multiple UAVr and LEO satellites on the same frequency band while using different frequencies for communication with GBS. Each UAVr is assumed to operate for a maximum of 30 minutes per flight, reflecting practical battery constraints in real-world deployments [17]. We will discuss the signal and channel models in the upcoming subsections.

Notational Convention: Scalars are written in regular font (e.g., $p_{i \leftarrow j}$, $\gamma_{i \leftarrow j}$), whereas all vectors and matrices are written in boldface (e.g., $\mathbf{h}_{i \leftarrow s}$, $\mathbf{n}_{i \leftarrow s}$, $\mathbf{u}_i$). Since each UAVr employs a single antenna, the satellite-to-UAVr channel $\hbar_{j \leftarrow s}$ and the corresponding received signal $r^{j \leftarrow s}$ are scalar quantities.

A. Signal model

This subsection presents the signal model for the LEO-assisted multiple UAVr-based communication framework. The proposed framework pertains to a dual-hop cooperative diversity system comprising an LEO satellite (s), multiple UAVr ($\mathbf{U}_j$), and ground users ($\mathbf{u}_i$), each equipped with L antennas, as illustrated in Fig. 1. The channel coefficients are defined as follows: $\mathbf{h}_{i \leftarrow s}$ represents the complex channel coefficients from the satellite to the lth antenna of the ground user, $\hbar_{j \leftarrow s}$ denotes the coefficients between the satellite and the UAVr, and $\mathbf{h}_{i \leftarrow j}$ corresponds to those between the UAVr and the ground user antennas.

Assuming that the satellite transmits a signal x_{sym} with an average power of P_s^{tx} during the first phase, the signal received at the UAVr from the satellite is given by

$$r^{j \leftarrow s} = \hbar_{j \leftarrow s} x_{\text{sym}} + n_{j \leftarrow s}.$$

The system employs a TDMA-based scheduling strategy in which each time slot serves exactly one scheduled ground user. Although the transmit power is indexed by user and UAVr indices for notational generality, at any given time slot, only the scheduled user UAVr pair is active. Consequently, only one transmit power variable is effective per slot, while all remaining power variables are inactive during that slot. In Phase I, the satellite transmits a single codeword intended for the scheduled user, which is received simultaneously by that user and by the associated UAVr. No intra-slot multi-user transmission occurs on either the satellite or UAVr links, and no bandwidth or power sharing among multiple users takes place within a time slot.

In contrast, the signal received directly from the satellite to the user is given by

$$\mathbf{r}^{i \leftarrow s} = \mathbf{h}_{i \leftarrow s} x_{\text{sym}} + \mathbf{n}_{i \leftarrow s}.$$

In the second phase, the satellite remains silent, and the UAVr retransmits a scaled version of the received signal from

the satellite in fixed-gain AF mode, with the received signal at the user expressed as

$$\begin{aligned}\mathbf{r}^{i\leftarrow j\leftarrow s} &= \mathbf{h}_{i\leftarrow j\leftarrow s}\,\mathcal{G}\left(r^{j\leftarrow s}\right) + \mathbf{n}_{i\leftarrow j\leftarrow s} \\ &= \mathbf{h}_{i\leftarrow j\leftarrow s}\,\mathcal{G}\hbar_{j\leftarrow s}x_{\text{sym}} + \mathbf{h}_{i\leftarrow j\leftarrow s}\,\mathcal{G}n_{j\leftarrow s} + \mathbf{n}_{i\leftarrow j\leftarrow s}.\end{aligned}$$

The above dual-hop cooperative communication framework at the user end is written as

$$\mathbf{r}^{\text{Tot}} = \mathbf{h}x_{\text{sym}} + \mathbf{n}, \tag{1}$$

where $\mathbf{r}^{\text{Tot}} = \begin{bmatrix}\mathbf{r}^{i\leftarrow s}\\ \mathbf{r}^{i\leftarrow j\leftarrow s}\end{bmatrix}$, $\mathbf{h} = \begin{bmatrix}\mathbf{h}_{i\leftarrow s}\\ \mathbf{h}_{i\leftarrow j\leftarrow s}\,\mathcal{G}\hbar_{j\leftarrow s}\end{bmatrix}$, $\mathbf{n} = \begin{bmatrix}\mathbf{n}_{i\leftarrow s}\\ \mathbf{h}_{i\leftarrow j\leftarrow s}\,\mathcal{G}n_{j\leftarrow s} + \mathbf{n}_{i\leftarrow j\leftarrow s}\end{bmatrix}$. The noise vectors $\mathbf{n}_{i\leftarrow s}$, $n_{j\leftarrow s}$, and $\mathbf{n}_{i\leftarrow j\leftarrow s}$ denote the L-dimensional AWGN at the ground user (first hop), the UAVr, and the ground user (second hop), respectively, and are modeled as $\mathcal{CN}(0,\sigma^2)$. The fixed AF relay gain at the UAVr is defined as $\mathcal{G}^2 = \frac{1}{|\hbar_{j\leftarrow s}|^2+\sigma^2}$, where $\hbar_{j\leftarrow s}$ denotes the satellite-to-UAVr channel coefficient and σ^2 is the AWGN variance. Although $\hbar_{j\leftarrow s}(t)$ is a random variable, its realization is assumed to be fixed within each time slot under the quasi-static fading model [31]; therefore, the AF relay gain $\mathcal{G}(t)$ is fixed per slot and adapts between slots as the channel evolves. This modeling ensures that the gain remains constant during AF operation based on slots, while allowing time-dependent power optimization through $p_{i\leftarrow j}(t)$ in multiple slots, consistent with the energy-efficiency objective. Although the UAVr operates as a fixed-gain AF relay, the transmit power $p_{i\leftarrow j}(t)$ is optimized on a per-slot basis subject to a maximum power constraint, as detailed in Section V.

B. Channel Model

This subsection discusses the channel between the LEO satellite and the user, the LEO satellite to the UAVr, and the UAVr to the user.

1) UAVr to User: The horizontal distance between the UAVr and the location of the user on the ground can be defined as (Fig. 1)

$$r_{i\leftarrow j}(t) = \sqrt{(x_j(t)-x_i)^2 + (y_j(t)-y_i)^2}. \tag{2}$$

Based on equation (2), the Euclidean distance between the UAVr and the ground user can be defined as

$$d_{i\leftarrow j}(t) = \sqrt{r_{i\leftarrow j}^2(t) + (h_j^{\text{Ur}}(t))^2}. \tag{3}$$

The path loss to the user is computed using the air-to-ground channel model from [32], based on line-of-sight (LoS) and NLoS conditions, given by

$$\begin{aligned}PL_{d_{i\leftarrow j}}^{\text{LoS}}(t) &= 20\log_{10}\left(\frac{4\pi f_c d_{i\leftarrow j}(t)}{c}\right) + \eta_{\text{LoS}},\\ PL_{d_{i\leftarrow j}}^{\text{NLoS}}(t) &= 20\log_{10}\left(\frac{4\pi f_c d_{i\leftarrow j}(t)}{c}\right) + \eta_{\text{NLoS}}.\end{aligned}$$

Here, η_{LoS} and η_{NLoS} are the additional mean losses due to LoS and NLoS communication links [33]; c is the speed of light in meters per second; and f_c is the carrier frequency in hertz. The corresponding probability of LoS signals from the UAVr to the ground user is given by

$$P_{d_{i\leftarrow j}}^{\text{LoS}}(t) = \frac{1}{1 + a\exp\left(-b\left(\frac{180}{\pi}\theta_{i\leftarrow j} - a\right)\right)},$$

where $\theta_{i\leftarrow j} = \tan^{-1}\left(\frac{h_j^{\text{Ur}}(t)}{r_{i\leftarrow j}(t)}\right)$ (in radians) is the elevation angle between the UAVr and the user, as shown in Fig. 1; a and b are constant factors that depend on different environmental conditions (rural, urban, dense urban, etc.). For $P_{d_{i\leftarrow j}}^{\text{LoS}}(t)$, the probability of NLoS signals from the UAVr to the ground user is given by $P_{d_{i\leftarrow j}}^{\text{NLoS}}(t) = 1 - P_{d_{i\leftarrow j}}^{\text{LoS}}(t)$. The channel gain $\mathbf{h}_{i\leftarrow j}$ between the UAVr and the user is defined as [34]

$$\begin{aligned}\mathbf{h}_{i\leftarrow j}(t) =& \mathfrak{g}_{i\leftarrow j}\left(\frac{4\pi f_c d_{i\leftarrow j}(t)}{c}\right)^{-\frac{\alpha_{\text{exp}}}{2}} \\ &\times 10^{-\frac{P_{d_{i\leftarrow j}}^{\text{LoS}}(t)\times PL_{d_{i\leftarrow j}}^{\text{LoS}}(t) + P_{d_{i\leftarrow j}}^{\text{NLoS}}(t)\times PL_{d_{i\leftarrow j}}^{\text{NLoS}}(t)}{20}},\end{aligned} \tag{4}$$

where $d_{i\leftarrow j}$ is the distance between the UAVr and the user, $\mathfrak{g}_{i\leftarrow j}$ denotes the channel gain that includes both small-scale fading and the effect of antenna gain, following the stochastic modeling convention, and α_{exp} denotes the path-loss exponent of the UAVr to user link. The average path loss of the signal from the UAVr to the ground user is computed as

$$\begin{aligned}PL_{d_{i\leftarrow j}}^{\text{Avg}}(t) &= P_{d_{i\leftarrow j}}^{\text{LoS}}(t)\times PL_{d_{i\leftarrow j}}^{\text{LoS}}(t) + P_{d_{i\leftarrow j}}^{\text{NLoS}}(t)\times PL_{d_{i\leftarrow j}}^{\text{NLoS}}(t)\\ &= \frac{\eta_{\text{LoS}} - \eta_{\text{NLoS}}}{1 + a\exp\left(-b\left[\frac{180}{\pi}\theta_{i\leftarrow j} - a\right]\right)} + 20\log_{10}\left(d_{i\leftarrow j}(t)\right) + \beta,\end{aligned} \tag{5}$$

where $\beta = 20\log_{10}\left(\frac{4\pi f_c}{c}\right) + \eta_{\text{NLoS}}$.We also neglect satellite interference due to its relatively low power compared to the desired signal strength for advanced IoT devices [35]. Thus, the SINR for the user associated with UAVr can be defined as

$$\gamma_{i\leftarrow j}(t/2) = \left(p_{i\leftarrow j}(t)\,|\mathbf{h}_{i\leftarrow j}(t)|^2\right)/\left(B_{i\leftarrow j}\,\sigma^2 + I_u(t)\right). \tag{6}$$

where $I_u(t) = \sum_{k=1,k\neq j}^{K} p_{i\leftarrow k}(t)\,10^{PL_{d_{i\leftarrow k}}^{\text{Avg}}(t)/10}$ is the aggregate interference from all UAVr $k \neq j$ at the user i, and $B_{i\leftarrow j}$ denotes the bandwidth allocated to the UAVr→user link. Here $(t/2)$ marks the phase (I/II) within the slot; all instantaneous quantities are evaluated at time t. Accounting for the two-phase schedule is handled later in the rate expression. To guarantee the QoS requirement, we impose $\gamma_{i\leftarrow j} \geq \gamma_{\text{th}}$, where γ_{th} is the predefined SINR threshold for successful signal transmission. The hovering power of UAVr as a function of its operational altitude h_j^{Ur} is calculated as

$$p_j^{\text{Hov}} = p_0(1+\Delta)e^{\varepsilon h_j^{\text{Ur}}/2}, \tag{7}$$

where p_0 is the power consumed by the serving UAVr during hover; Δ and ε are constants; and h_j^{Ur} is the altitude of the UAVr. The exponential form adopted from [14] originates from an aerodynamic drag model, which inherently reflects altitude-related resistance and static environmental factors such as air

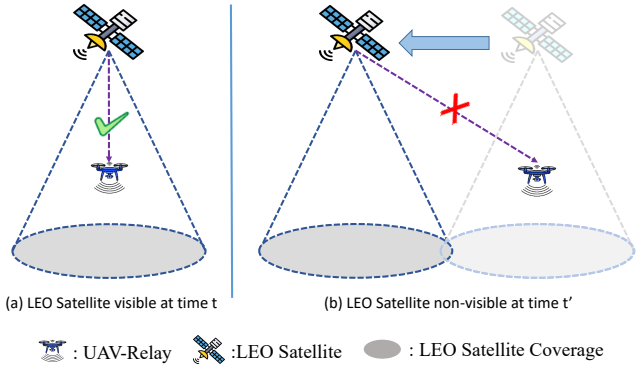

Fig. 2: Illustration of LEO satellite visibility states. LEO satellites travel at high orbital speeds (typically 7.8 km/s [36]), causing rapid changes in visibility to ground or aerial nodes.

density. The hovering altitude of the UAVr corresponding to its hovering power, derived from (7), is given by

$$h_j^{\mathrm{Ur}} = \frac{2}{\varepsilon} \ln\left(\frac{p_j^{\mathrm{Hov}}}{p_0(1+\Delta)}\right). \tag{8}$$

Since the altitude of UAVr is fixed at a regulatory-compliant 100 m in all schemes, the hover power acts as a constant offset in total energy consumption. Therefore, this constant does not alter the results of relative performance or the conclusions drawn from our comparative analysis.

2) LEO Satellite to UAVr and User : Due to the high-speed orbits of LEO satellites and their limited visibility periods to multiple UAVr, a satellite constellation is essential to ensure continuous backhauling capabilities. Orbital pass periods during which LEO satellites are directly visible to multiple UAVr are a critical factor influencing backhaul efficiency [37]. Since LEO satellites are not geostationary, their movements must be analyzed before evaluating the system's performance. We assume that each UAVr is continuously associated with an LEO satellite. For computational convenience regarding satellite-Earth geometries, we model the satellite following a circular orbit. The connection between a UAVr and an LEO satellite is represented by a visibility variable $V_{j\leftarrow s}(t)$ at the time interval t, as defined in [38].

$$V_{j\leftarrow s}(t) = \begin{cases} 1 & \text{if } \cos\left(\frac{2\pi \mathrm{t}}{T_s} - \theta_p\right) \geq \frac{R_E^2 + r_{\mathrm{EC}}^2 - d_{\mathrm{SR}}^2}{2R_E r_{\mathrm{EC}}} \\ 0 & \text{otherwise.} \end{cases} \tag{9}$$

To avoid potential ambiguity, satellite visibility is evaluated at the beginning of each time slot and assumed constant over the slot duration. If the LEO satellite is visible at time t, then $V_{j\leftarrow s}(t) = 1$; otherwise, $V_{j\leftarrow s}(t) = 0$ [39], as shown in Fig. 2. Similarly, the visibility variable from the user to the LEO satellite, $V_{i\leftarrow s}(t)$, is determined in the same manner as in equation (9). Here, $d_{\mathrm{SR}} \geq d_{j\leftarrow s}$ represents the slant range corresponding to the minimum elevation angle, R_E is the radius of the Earth, r_{EC} is the distance between the LEO satellite and the Earth's center, θ_p is the polar angle of the UAVr, and T_s is the orbital period of the satellite. It is assumed that the handover between LEO satellites and multiple UAVr occurs through advanced handover (HO) schemes, such as guaranteed and prioritized HO; therefore, frequent handovers due to LEO satellite movement do not affect the reliability of the data transmission [40]. We assume that the links between the LEO satellite and the UAVr or the user follow the shadowed-Rician fading (SRF) model. The channel gain from the satellite to the UAVr is expressed as [34]:

$$\hbar_{j\leftarrow s} = \sqrt{\mathfrak{g}^{\mathrm{avg}} d_{j\leftarrow s}^{-\alpha_{\mathrm{exp}}^2}}, \tag{10}$$

where the term $\mathfrak{g}^{\mathrm{avg}}$ represents the average antenna gain between the LEO satellite and the UAVr/user and captures the overall gain and fading behavior in the satellite communication links. $d_{j\leftarrow s}$ is the distance between the satellite and the j^{th} UAVr, and α_{exp}^2 is the path loss exponent from the satellite to the UAVr. The term $g^{\mathrm{avg}} \sim \mathrm{SR}(\wp, \Im, \varnothing)$ represents the SRF component with an average power of the direct signal $\wp$, half of the average power of the scattered portion $\Im$, and the Nakagami-m fading component $\varnothing$.

The instantaneous SNR for the satellite-to-UAVr link, based on the satellite visibility criterion in (9), is given as

$$\gamma_{j\leftarrow s}(t/2) = (V_{j\leftarrow s}(t)\, P_s^{\mathrm{tx}}\, |\hbar_{j\leftarrow s}(t)|^2)/(B_{j\leftarrow s}\, \sigma^2\,). \tag{11}$$

Same convention as Eq. (6): $(t/2)$ is a phase indicator; instantaneous terms are taken at time t. Similarly, the channel coefficient for the satellite-to-user link is modeled as

$$\mathbf{h}_{i\leftarrow s}(t) = \sqrt{\mathfrak{g}^{\mathrm{avg}}\, d_{i\leftarrow s}(t)^{-\alpha_{\mathrm{exp}}}},$$

and the corresponding SNR is

$$\gamma_{i\leftarrow s}(t/2) = V_{i\leftarrow s}(t)\, \frac{P_s^{\mathrm{tx}} \left\|\mathbf{h}_{i\leftarrow s}(t)\right\|^2}{B_{i\leftarrow s}\, \sigma^2 + I_u(t)}. \tag{12}$$

Here, P_s^{tx} is the satellite transmission power, $B_{i\leftarrow s}$ denotes the bandwidth allocated to the satellite-to-user link during its active phase, and $(t/2)$ marks the phase (I/II) within the slot; instantaneous quantities are evaluated at time t. It is noted that the satellite–UAVr and satellite–user distances vary with orbital motion across time intervals, and this variation is incorporated into the SINR calculation through (9), (11), and (12). UAVr positions are assumed constant within a time slot for tractability.

3) GBS to User : The user is assumed to experience independent Rayleigh fading when associated with the GBS. In each time interval t, the channel coefficient is represented as:

$$\mathbf{h}_{i\leftarrow G}\,(t) = \mathfrak{g}_{i\leftarrow G}\,(r_{i\leftarrow G}\,(t))^{-\alpha_{\mathrm{exp}}}. \tag{13}$$

Here, $\mathfrak{g}_{i\leftarrow G}$ denotes the channel gain that captures both the antenna gain and small-scale Rayleigh fading, modeled as a complex Gaussian random variable, i.e., $\mathfrak{g}_{i\leftarrow G} \sim \mathcal{CN}(0,1)$. The variable $r_{i\leftarrow G}$ represents the horizontal distance between the user and the GBS. Thus, the SNR for the user associated with the GBS can be defined as follows:

$$\gamma_{i\leftarrow G}\,(t) = \frac{P_G^{\mathrm{tr}} \|\mathbf{h}_{i\leftarrow G}\,(t)\|^2}{B_{i\leftarrow G}\sigma^2}. \tag{14}$$

The GBS transmits at a fixed power P_G^{tr} for terrestrial communications. To maximize total network capacity while ensuring fairness, UAVr/satellite links are utilized only when the GBS

cannot accommodate additional users. We define $\delta_{i\leftarrow G}(t)$ as a binary indicator for the user at time t, indicating whether the user meets the load conditions under GBS coverage:

$$\delta_{i\leftarrow G} = \begin{cases} 1, & \text{if} \quad |\Omega_G| \le \omega_G^{\max} \\ 0, & \text{otherwise.} \end{cases} \tag{15}$$

Here, Ω_G and $\omega_G^{\max}$ show the current user associated with GBS and the maximum user association capacity of GBS.

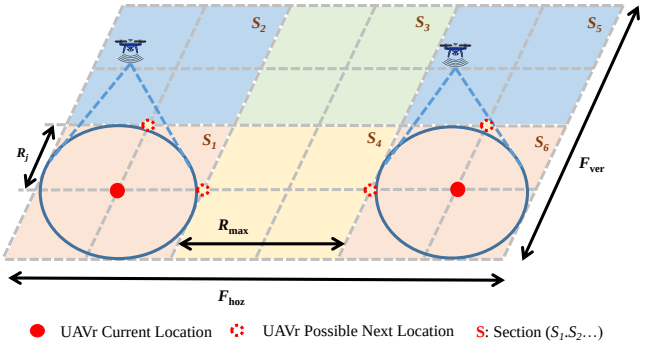

Fig. 3: Illustration of the UAVr mobility model. Each UAVr provides circular coverage with radius R_j (blue disk), while the rectangular grid represents logical subdivisions of the GBS area for hotspot tracking and UAVr displacement planning. The grid does not imply rectangular coverage but is used for section-wise traffic analysis and decision-making. The UAVr selects its next location within its circular reach based on traffic demand.

IV. UAVr Deployment and Signal Combining

When GBS cannot meet the QoS requirements of network users, the proposed AMUD approach first involves intelligently deploying multiple UAVr over the hotspot area and then collaboratively serving the users with the help of the LEO satellite. In this section, we first analyze the adaptive placement of multiple UAVr, followed by a signal-combining analysis of the LEO satellite and multiple UAVr.

A. UAVr Coverage Analysis

In this subsection, we discuss the deployment of multiple UAVr through the proposed AMUD framework. As illustrated in Fig. 3, the coverage area of a UAVr is considered circular with a radius of R_j. Let the terrestrial area under GBS coverage be denoted as A, with dimensions $F_{\text{hoz}} \times F_{\text{ver}}$. The area A is subdivided into smaller sections that represent the coverage of multiple UAVr, denoted S_A, where $S_A < A$. A key objective of the proposed AMUD framework is to deploy multiple UAVr in sectors experiencing heavy traffic. Furthermore, intelligent user association must be performed to ensure that each user connects to the most relevant access point. A user is considered to be within coverage if it is located within a distance of at most R_j from the center of the coverage region, i.e.,

$$\delta_{i\leftarrow j} r_{i\leftarrow j}^2(t) \le R_j^2(t). \tag{16}$$

We further modify the above equation as follows [41],

$$r_{i\leftarrow j}^2(t) \le R_j^2(t) + M(1-\delta_{i\leftarrow j}). \tag{17}$$

Here, M is a large constant, indicating that the user is far from the access point when $\delta_{i\leftarrow j} = 0$. The equation above signifies user association when $\delta_{i\leftarrow j} = 1$. Thus, $\delta_{i\leftarrow j} \in \{0, 1\}$ serves as an indicator function that represents the association of a user with an access point. Mathematically, it can be expressed as follows:

$$\delta_{i\leftarrow j} = \begin{cases} 1, & \text{if, } r_{i\leftarrow j}^2(t) \le R_j^2(t) \\ 0, & \text{otherwise.} \end{cases} \tag{18}$$

In a multiple-UAVr deployment framework, the multiple UAVr traverse the entire network region while hovering at the same height. Therefore, maintaining a safe distance is crucial to prevent collisions between multiple UAVr. A collision between two UAVr occurs when their distance is $d_{j\leftarrow j'} = 0$ [17]. To mitigate this risk, the proposed AMUD framework incorporates a safe distance parameter $R_{\max}$ among multiple UAVr, ensuring that $d_{j\leftarrow j'} \ge R_{\max}$, where j and j' denote different UAVr (Fig. 3).

For tractability, UAVr repositioning within a time slot is assumed instantaneous, representing the most responsive case; in practice, repositioning delays may slightly reduce achievable gains. The following subsection discusses the space-time CD signal combining strategy within the proposed AMUD framework.

B. Cooperative Diversity Technique

Following the adaptive deployment of UAVr discussed in the previous subsection, we would like to explore the combined CD-based signal at the ground user within the proposed AMUD framework. The user is assumed to possess L antennas. In this scenario, the UAVr is retransmitting the signal from the LEO satellite to the destination nodes, the ground user [42].

Communication from a user through the LEO satellite-aided UAVr occurs as follows. The proposed AMUD approach combines the signals received by the user in two phases. The LEO satellite and UAVr signals to the ground user arrive via time division multiple access (TDMA) protocols from Phase I to Phase II, as illustrated in Fig. 1. During Phase I, the source (i.e., LEO satellite) simultaneously transmits a signal to both the relay node (i.e., UAVr) and the destination node (i.e., ground user). Subsequently, in Phase II, using the AF protocol, the UAVr retransmits the source signal to the user while the satellite remains silent. Additionally, we assume that no information exchange occurs between a UAVr and a LEO satellite between Phase I and Phase II while operating in time division duplex mode; therefore, the total time slot is two [43]. Satellite and UAVr signals are assumed to be perfectly in synchronization with the user [12]. This synchronization is achieved through timing calibration aided by terrestrial control stations and timing advance adjustments based on device locations [44]. It should be noted that the AF protocol offers a more straightforward implementation and lower complexity than DF. Recognizing this advantage, our framework leverages AF for efficient signal relaying [42]. AF relays are adopted here for their low latency and simple implementation compared to DF [31], though they inherently forward both signal and noise. Our SINR-weighted combining (9)–(12) assigns lower weights to noisier relay paths, mitigating noise amplification, while the cooperative diversity

between the satellite and UAVr links further suppresses residual noise.

Let $\mathbf{w} = \left(w_{1_1}, w_{1_2}, \ldots, w_{1_L}, w_{2_1}, w_{2_2}, \ldots, w_{2_L}\right) \in \mathbb{C}^{2L}$ be a weighting vector used to combine $2L$ received signals from the LEO satellite and the UAVr as defined in equation (1) Then, using the CD receiver with the weighting vector $\mathbf{w}^\dagger$, we can express the combined output $\mathbf{w}^\dagger \mathbf{r}_{\mathrm{s}}^{\mathrm{Tot}}$ to the user as:

$$\mathbf{w}^\dagger \mathbf{r}_{\mathrm{s}}^{\mathrm{Tot}} = \underbrace{\mathbf{w}^\dagger \mathbf{h} \mathbf{x}_{\mathrm{sym}}}_{\text{Signal}} + \underbrace{\mathbf{w}^\dagger \mathbf{n}}_{\text{Noise}}. \tag{19}$$

where the superscript $(\cdot)^\dagger$ indicate the transpose of vector $\mathbf{w}$. In the presence of complete CSI at the destination, the instantaneous SINR at the user can be expressed as

$$\gamma_{\mathrm{AF}}(\mathbf{w}) = P_s^{\mathrm{tx}} \frac{\mathbf{w}^\dagger R_{\mathrm{k}} \mathbf{w}}{\mathbf{w}^\dagger \mathscr{R}_{\mathrm{n}} \mathbf{w}} \tag{20}$$

This expression models the optimal combination on the receiver side under a fixed AF relay gain $\mathcal{G}(t)$, and does not imply any adaptive gain control on the UAVr.

Proof. Please refer to Appendix A. □

Taking the derivative of (20) to the weight vector $\mathbf{w}$ [45], we get the optimal beamforming weight vector in a dual-hop cooperative communication system given by

$$\mathbf{w}_{\mathrm{opt}} = c_r \mathbf{h}' = c_r \mathscr{R}_n^{-1} \mathbf{h}. \tag{21}$$

Hence, the maximum SINR in a dual-hop amplify and forward communication system is given as

$$\gamma_{\mathrm{AF,\,max}}^{\mathrm{CD}}(\mathbf{w}_{\mathrm{opt}}) = \gamma_{i \leftarrow s} + \frac{\gamma_{j \leftarrow s} \gamma_{i \leftarrow j}}{\gamma_{i \leftarrow j} + \varsigma}. \tag{22}$$

Proof. Please refer to Appendix B. □

To indicate whether the user is associated with the $\mathbf{U}_j$-th UAVr, the indicator function $\delta_{i \leftarrow j}$ is modified to incorporate the QoS and coverage constraints of the user.

$$\delta_{i \leftarrow j} = \begin{cases} 1, & \text{if, } \left(\gamma_{\mathrm{AF,\,max}}^{\mathrm{CD}}(t) \geq \gamma_{\mathrm{th}}\right) \wedge \left(r_{i \leftarrow j}^2(t) \leq R_j^2(t)\right) \\ 0, & \text{otherwise.} \end{cases} \tag{23}$$

It is assumed that each user can only connect to one UAVr at a time for fair user association, and such a constraint is written as

$$\sum_{j=1}^{K} \delta_{i \leftarrow j} = 1, \tag{24}$$

C. Total Capacity Calculation

In the two-phase TDMA cooperative scheme illustrated in Fig. 1, Phase I corresponds to satellite transmission and Phase II to UAVr forwarding, with each phase occupying half of the duration of the slot. The achievable data rate (in Mbps), obtained from (22) based on Shannon's theorem, is expressed as

$$c_{\mathrm{AF,max}}^{\mathrm{CD}}(t) = (1/2)\, B_{i \leftarrow j}\, \log_2\!\left(1 + \gamma_{\mathrm{AF,max}}^{\mathrm{CD}}(t)\right) \delta_{i \leftarrow j}(t). \tag{25}$$

The factor $1/2$ reflects the two equal-duration phases in the schedule. $B_{i \leftarrow j}$ denotes the bandwidth allocated to the active downlink (e.g., UAVr→user) during its assigned phase; analogous definitions apply for other links when composing $\gamma_{\mathrm{AF,max}}^{\mathrm{CD}}(t)$. According to equations (15) and (25), the data transmission rate achievable by users associated with LEO satellites through UAVr is

$$C_j(t) = \sum_{i \in \Omega_j, \forall i \in \{1,2,\ldots,N_{\mathrm{U}}\}} c_{\mathrm{AF,max}}^{\mathrm{CD}}(t), \tag{26}$$

where $\Omega_j = \max(0, |\Omega_{\mathrm{Tot}}| - \omega_G^{\max})$ is the set of users associated with the collaboration between the UAVr and the LEO satellite, Ω_{Tot} is the total set of users in the system, $\omega_G^{\max}$ is the maximum user association capacity of the GBS and N_{U} is the number of users collaboratively by the UAVr and LEO satellite. The achievable data rate for a user associated with the GBS, as given by equation (14), is

$$c_{i \leftarrow G}(t) = B_{i \leftarrow G} \log_2(1 + \gamma_{i \leftarrow G}(t)) \cdot \delta_{i \leftarrow G}(t), \tag{27}$$

where $B_{i \leftarrow G}$ is the bandwidth (MHz) allocated to the GBS-associated user. The data transmission rate of the GBS (27) serving its associated users is calculated as follows.

$$C_G(t) = \sum_{i \in \Omega_G, \forall i \in \{1,2,\ldots,N_{\mathrm{G}}\}} c_{i \leftarrow G}(t), \tag{28}$$

where Ω_G is the set of users associated with GBS and N_{G} is the number of users served by GBS.

From (26) and (28), the total capacity of the network is given as

$$C^{\mathrm{Tot}}(t) = \sum_{j=1}^{K} C_j(t) + C_G(t). \tag{29}$$

The total power consumption of the downlink system, including the communication power of the UAVr, the hovering power of the UAVr, the transmission power of the satellite, and the transmission power of the GBS, is given by

$$p^{\mathrm{Total}}(t) = \underbrace{\sum_{j=1}^{K} \left(\sum_{i=1}^{N_U} p_{i \leftarrow j}(t) + p_j^{\mathrm{Hov}}(t) \right)}_{\text{UAVr Power (Comm.+Hover)}} + \underbrace{P_s^{\mathrm{tx}}(t)}_{\text{LEO Power}} + \underbrace{\sum_{i=1}^{N_G} P_G^{\mathrm{tr}}(t)}_{\text{GBS Power}} \tag{30}$$

To clarify the GBS power model, we assume a fixed transmit power spectral density (PSD), resulting in a constant transmit power P_G^{tr} for each user's allocated bandwidth. Consequently, the total power consumption of the GBS, denoted as P_G^{tr}(t), increases linearly with the number of users associated with the time interval t. This relationship is explicitly captured in 30, ensuring that the model accounts for both operational overhead and dynamic user load. From (29) and (30), we can derive the total energy efficiency as

$$E^{\mathrm{Tot}}(t) = \frac{C^{\mathrm{Tot}}(t)}{p^{\mathrm{Total}}(t)} \tag{31}$$

We introduce a capacity fairness constraint to ensure user fairness in a multi-access point framework. We use Jain's fairness index (JFI) [46] metrics to measure performance and provide fair communication services to different users in the deployed UAVr-aided hybrid space-terrestrial network. Fairness

among users is demonstrated using JFI. This index, denoted by ξ, serves as a fairness metric and is defined as:

$$\xi = \frac{\left(\sum_{i=1}^{N_U} c_{\text{AF,max}}^{\text{CD}} + \sum_{i=1}^{N_G} c_{i\leftarrow G}\right)^2}{N\left(\sum_{i=1}^{N_U} {c_{\text{AF,max}}^{\text{CD}}}^2\right) + N\left(\sum_{i=1}^{N_G} {c_{i\leftarrow G}}^2\right)}. \tag{32}$$

The index value ξ is in the range $[0, 1]$. A value of one indicates equal data rates among different network users. A higher value of the fairness index corresponds to smaller differences between the total data rates allocated to the users. In the upcoming section, we formulate a network capacity maximization problem that incorporates the system and fairness constraints introduced in this section.

V. Energy Efficiency Maximization Formulation

In this work, our objective is to improve the total energy efficiency of the network using the proposed AMUD approach, which involves the adaptive placement of multiple UAVr at desired locations, followed by intelligent signal combining from the LEO satellite and multiple UAVr. Given the limited onboard battery capacity of multiple UAVr, which affects hovering time and communication efficiency, maximizing energy efficiency is crucial, especially in critical scenarios such as disaster response and temporary communications [14]. Thus, we optimize user association and transmit power allocation to maximize total energy efficiency. The formulation of the problem, constrained by the minimum data rate requirements as defined in equations (25) and (27), user association specifications, and fairness considerations, is discussed below from equation (31).

$$\max_{\delta_{i\leftarrow j}(t), p_{i\leftarrow j}(t)} \sum_{i=1}^{T} E^{\text{Tot}}(t) \tag{33}$$

The multi-objective problem is scalarized using an α-weighted sum of the normalized total capacity and normalized total energy efficiency, with fairness and QoS constraints enforced as hard constraints.

subject to (15) (22), (23), (24), (25), (27),

$$0 \le p_{i\leftarrow j} \le p_{\max}, \tag{34a}$$
$$0 \le |\Omega_j| \le \omega_j^{\max}, \tag{34b}$$
$$0 \le |\Omega_G| \le \omega_G^{\max}, \tag{34c}$$
$$r_{i\leftarrow j}^2(t) \le R_j^2(t),$$
$$\delta_{i\leftarrow j} \in \{0, 1\}, \ \forall i \in \Omega_j, \tag{34d}$$
$$\delta_{i\leftarrow G}(t) + \delta_{i\leftarrow j}(t) = 1 \ \forall i, \tag{34e}$$
$$\xi \ge \xi_{\text{th}}. \tag{34f}$$
$$\mathbf{U}_j(t), \forall t \in \{1, T\}. \tag{34g}$$

The restriction (34a) specifies the transmission power limit for each UAVr serving associated users within its coverage area, influenced by factors such as the altitude of the UAVr, the duration of service and the number of users. Constraints (34b) and (34c) restrict user associations with the UAVr and GBS, respectively. The system identifies candidate configurations, including UAVr locations $\mathbf{U}_j^{\text{2D}}$ and optimal coverage radius R_j, based on relationships defined in equation (34d), derived from equation (23). The constraint (34e) ensures that each user is associated with either the GBS or the UAVr. The constraint (34f) ensures a fair distribution of users among multiple UAVr and GBS, with the fairness constraint $\xi \ge \xi_{\text{th}}$ directly applied to the feasible set, ensuring that fairness is maintained independently of the scalarized objective. The constraint (34g) specifies the initial and final location based on t.

The maximum path loss of each user, $PL_{d_{i\leftarrow j}}^{\max}$, is a fixed value in the system. Using this maximum path loss, we calculate the optimal angle θ_j^{opt} by solving the non-linear partial differential equation $\frac{\partial r_{i\leftarrow j}}{\partial \theta_j^{\text{opt}}} = 0$ from the equation (5), as expressed in [32].

$$\frac{\pi \tan\theta_j}{9\ln(10)} + \frac{abA\exp\left(-b\left[\frac{180}{\pi}\theta_j - a\right]\right)}{\left(a\exp\left(-b\left[\frac{180}{\pi}\theta_j - a\right]\right) + 1\right)^2} = 0. \tag{35}$$

With the optimal angle obtained θ_j^{opt}, if the altitude of the $\mathbf{U}_j$-th UAVr, denoted as h_j^{Ur}, is given, the corresponding coverage radius R_j can be derived using the relationship.

$$\theta_j = \tan^{-1}\left(h_j^{\text{Ur}}/R_j\right), \tag{36}$$

and θ_j is set to the optimal angle θ_j^{opt}. Since the maximum altitude $h_{\max}$ is a predefined constraint, we can use equation (36) to determine the maximum coverage radius $R_{\max}$ provided by a UAVr. Additionally, the maximum allowable LoS distance (Euclidean distance) for the $\mathbf{U}_j$-th UAVr will be

$$d_{\max} = R_{\max}\sec\theta_j^{\text{opt}}. \tag{37}$$

A. The NP-Hardness

In this subsection, we prove that the problem (33) is NP-hard. To establish this, we first relax certain constraints, specifically the fixed user association, and transform problem (33) into a related problem, denoted as (38). Subsequently, by establishing that the problem (38) is NP-hard or NP-complete, we can conclude that the original problem (33) is NP-hard. The new problem (38) is formally defined as follows.

$$\max_{p_{i\leftarrow j}(t)} E^{\text{Tot}} \tag{38}$$

s.t. (22),(23),(24), (25), (34a), (34b), (34c), (34d), (34f) (34g). Note: The constraints discussed are (33). Using the above statement, we deduce the following theorem.

Theorem 1. *The original problem* (33) *is NP-hard.*

Proof. By relaxing the constraints of user association and assuming that all multiple UAVr serve a fixed set of users, problem (38) has been proved NP-hard, as shown in [47]. Thus, the NP-hardness of the problem (38) implies that the original problem in equation (33) is also NP-hard. The NP-hardness of the original problem in equation (33) follows by reduction to a known NP-hard problem [47], with the relaxed form in equation (38) preserving the core combinatorial difficulty and guiding the heuristic design in Section V. □

However, optimizing transmission power with a fixed user association becomes significantly more manageable [47]. Therefore, in the following sections, we introduce an algorithmic approach based on AMUD to optimize the transmission power of UAVr $p_{i\leftarrow j}$ by fixing the association variable $\delta_{i\leftarrow j}$.

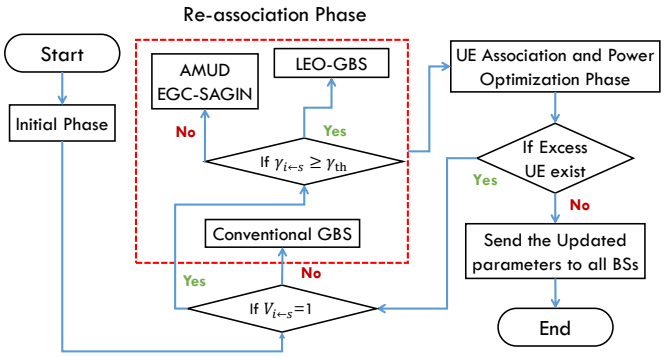

Fig. 4: The flowchart of the AMUD framework.

VI. The Proposed AMUD Framework

This section presents the main concept and an overview of the proposed AMUD method. Following this, we will describe the AMUD procedure in detail. Finally, we will discuss the key aspects of our proposed design.

A. Main Idea

The proposed AMUD framework addresses the problem of maximization of energy efficiency (33) while ensuring user fairness (32) and satisfying the minimum data rate constraints (25) for all users within the coverage region. The primary objective is to improve overall network capacity and energy efficiency through the intelligent and cooperative deployment of multiple UAVr in coordination with LEO satellites. The design intentionally follows a sequential and opportunistic trigger strategy, ensuring that the most critical issues, such as NLoS mitigation and uneven user distribution, are addressed first before transitioning to network fine-tuning through power optimization. This ordering prevents premature or redundant actions, resulting in a more robust and resource-efficient operation. The criteria used in each phase are derived directly from the constraints and objectives in (14), (28), and (32)–(33), ensuring that the logic is grounded in first-principles optimization rather than heuristic rules. Extensive simulations under varying traffic patterns, congestion levels, and satellite visibility conditions confirmed that these criteria consistently yield stable and robust performance. The AMUD framework is structured into three sequential operational phases, illustrated in Fig. 4, as follows:

1) **Initial Phase:** The CCS initializes the system with predefined parameters, including the location of the ground user and the states of association of the GBS. Assesses current network load and identifies user congestion patterns by evaluating surplus GBS associations (Ω_G^{Ex}) and UAVr sector user densities ($\omega_j^{\max}$). This initialization is executed once prior to the iterative process (Fig. 5(a)).
2) **Re-association Phase:** In this phase, the CCS dynamically re-assigns users based on GBS overload or UAVr sector density. Specifically, if $\omega_j^{\max} > 0$ or $\Omega_G^{\text{Ex}} > 0$, and satellite visibility conditions allow, users are reassigned to appropriate schemes among four alternatives:
   - **AMUD-SAGIN:** Adaptive UAV deployment is activated when the satellite is visible ($V_{i\leftarrow s} = 1$), but the SINR is below the threshold ($\gamma_{i\leftarrow s} < \gamma_{\text{th}}$).
   - **EGC-SAGIN:** Equal Gain combination is invoked under the same conditions ($V_{i\leftarrow s} = 1$, $\gamma_{i\leftarrow s} < \gamma_{\text{th}}$) to enhance signal reliability through cooperative diversity.
   - **LEO-GBS only:** If both visibility and SINR requirements are satisfied ($V_{i\leftarrow s} = 1$, $\gamma_{i\leftarrow s} \geq \gamma_{\text{th}}$), a direct LEO-GBS link is established.
   - **GBS-only:** If the satellite is not visible ($V_{i\leftarrow s} \neq 1$), terrestrial fallback connectivity is used through the conventional GBS association.

   This adaptive selection ensures reliable connectivity and optimized load distribution based on current link quality and topology (Fig. 5(b)). Unlike conventional reactive approaches, this phase is governed by an *a priori* decision logic that systematically evaluates satellite visibility and congestion states before triggering UAVr deployment, enhancing robustness and minimizing unnecessary re-associations.
3) **User Association and Power Optimization Phase:** Following the re-association phase, the CCS performs joint user association and transmit power optimization. This iterative process continues until all surplus users are efficiently reassigned and the optimal power allocation for each UAVr is determined. The final configurations are then distributed to the UAVr nodes for deployment and operation (Fig. 5(c)).

B. Proposed Algorithm

Algorithm 1 outlines the pseudo-code for the main procedure of the proposed AMUD approach, executed by the CCS. A detailed explanation of each step within the AMUD procedure is provided below:

- Lines 1 to 4: These lines correspond to the initialization phase, where the CCS prepares temporary matrices to store data required for subsequent re-association and optimization decisions.
- Line 5: The CCS evaluates whether it is overloaded by iterating through a for loop.
- Line 6: The CCS employs a while-loop system to monitor excess users. If $\Omega_G^{\text{Ex}} > 0$ or $\omega_j^{\max} > 0$, and if $V_{j\leftarrow s} = 1$ while $\gamma_{i\leftarrow s} < \gamma_{\text{th}}$, the CCS re-associates excess users from the overloaded GBS to the LEO satellite-assisted UAV. This process continues until conditions $\Omega_G^{\text{Ex}} = 0$ and $\omega_j^{\text{Max}} = 0$ are satisfied.
- Line 7: The CCS selects i^* from Ω_G, identifying the sector with user-generated hotspots where $\omega_j^{\text{Max}} > 0$ and $\Omega_G^{\text{Ex}} > 0$. A corresponding UAV is then activated and deployed to serve the selected users i^* with CCS support.

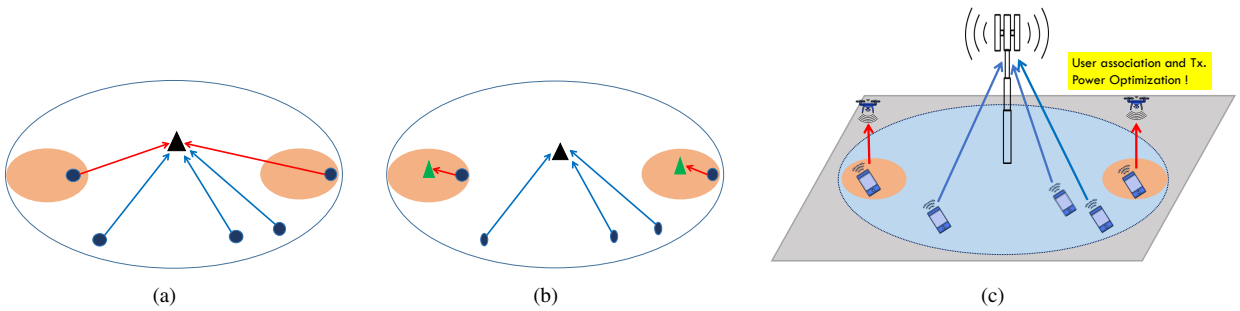

(a) (b) (c)

Fig. 5: The AMUD framework is visualized in 2D and 3D, showcasing phases: (a) Initial phase, (b) Re-association phase, and (c) User association and power optimization phase. Users are depicted as blue dots, GBS centers as black triangles, UAVr centers as green triangles, hotspots as orange-shaded areas, GBS coverage as blue circles, and UAVr coverage as orange-shaded circles. Arrows indicate user associations. For small-scale instances where exhaustive search is computationally feasible, the proposed heuristic achieves results within 5% of the optimal solution in tested scenarios, confirming its near-optimal performance in representative conditions.

- Lines 8 to 27: After re-associating users, a for-loop optimizes the transmit power of each UAVr with the assistance of the CCS.
- Line 10: The Euclidean distance is calculated between the j-th UAVr and the i-th user.
- Line 11: The path loss between the j-th UAVr and the i-th user is updated based on the changes in distance, $d_{i\leftarrow j}$, using equation (5).
- Line 12: The minimum required transmit power $p_{i\leftarrow j}^{\min}$ is determined to ensure the SINR value defined in equation (6) for the i-th user.
- Line 13: The optimal transmission power $p_{i\leftarrow j}$ is selected to maximize the total energy efficiency E^{Tot} from equation (31), ensuring that it adheres to the transmission power constraints.
- Lines 14 to 22: These lines verify that the transmission power constraints are met, followed by updating the transmission power values $p_{i\leftarrow j}$ at line 23.
- Line 28: The CCS checks for hotspot mobility and adaptively deploys multiple UAVr, ensuring a safe collision-free distance between them.
- Final Step: The CCS transmits updated parameter sets, Ω and P, to all UAVr for deployment adjustments.

In the upcoming section, we will discuss the simulated results alongside inferences and observations.

VII. Results and Discussion

This section presents the simulation results of the proposed AMUD framework by evaluating the optimization problem formulated (33) in terms of three key performance metrics: total network capacity, energy efficiency, and capacity fairness. Simulations were performed in MATLAB R2020b for an urban environment with randomly distributed users and varying levels of GBS overload (i.e., excess users). The performance of the proposed AMUD–SAGIN framework is compared with three representative benchmark schemes. Equal-gain combining-based SAGIN (EGC–SAGIN), a satellite-assisted terrestrial network that uses only LEO satellites and GBS (LEO–GBS), and a conventional GBS–only network. A detailed description of these baseline schemes is provided in Subsection VII-A.

TABLE III: Simulation Parameters

Parameter	Symbol	Value
Maximum path loss	$PL_{d_{i\leftarrow j}}^{\max}$	119 dB
Carrier frequency	f_c	2.4 GHz
LEO Satellite Altitude	h_{s}	1000 km
UAVr Service Altitude	h_j^{Ur}	100 m
GBS Coverage Area	$F_{\text{hoz}} \times F_{\text{ver}}$	1×1 km
Allocated Bandwidth	$B_{i\leftarrow j}, B_{i\leftarrow s}, B_{i\leftarrow G}$	20 MHz
Number of UAVr	K	2
Path loss exponent	α_{exp}	2
Total Number of Users	N	400
Max Associations at UAVr	$\omega_j^{\max}$	200
Max Associations at GBS	$\omega_G^{\max}$	100
SINR Threshold	γ_{th}	3 dB
Hovering Power	p_j^{Hov}	58 W
UAVr Transmission Power	$p_{\max}$	20 dBm
LEO Transmission Power	P_s^{tx}	50 dBm
GBS Transmission Power	P_G^{tx}	40 dBm

To comply with the real-world UAVr regulations in Taiwan, the UAVr altitude is fixed at 100 m, which is the legal height limit for low-altitude UAVr operations [48]. The simulation adopts the air-to-ground urban channel parameters $(a, b, \eta_{\text{LoS}}, \eta_{\text{NLoS}}) = (9.61, 0.16, 1, 20)$, based on the empirical model in [32]. The system bandwidth of 20 MHz and the noise power of -174 dBm/Hz follow standard values commonly used in recent UAVr and satellite communication studies [14]. Transmission power settings, user population, and GBS/UAVr association limits are selected based on configurations from the existing SAGIN literature to ensure a fair and realistic evaluation environment. The simulation parameters, including the carrier frequency f_c, the transmit power of the UAVr $p_{\max}$, and the thresholds of user association $\omega_{\max}$, are summarized in Table III.

A. Benchmark Schemes for Comparison

To evaluate the performance of the proposed AMUD framework, we compare it with the following three benchmark schemes under identical simulation settings:

- **AMUD–SAGIN:** This scheme combines the SINRs from the satellite–user and UAVr–user links using a weighted approach that prioritizes stronger links, as described in

Algorithm 1 AMUD Framework Workflow

Input:

$\omega_j^{\max}$: the maximum associations per UAVr;
$\omega_G^{\max}$: the maximum associations of GBS;
h_j^{Ur}: the altitude of UAVr (8);
$\mathbf{E} = \{u_1, \ldots, u_i, \ldots, u_N\}$: the set of users' horizontal locations, where $1 \leq \forall i \leq N$;
$\mathbf{U} = \{U_1, \ldots, \mathbf{U}_j, \ldots, U_K\}$: the set of UAVr' horizontal locations,;
$\mathbf{\Omega} = \{\mathbf{\Omega}_1, \ldots, \mathbf{\Omega}_K\}$: UAVr' association mapping;
$\mathbf{\Omega_j}$: the set of users associated with the j-th UAVr;
$|\mathbf{\Omega_j}|$: the number of users associated with the j-th UAVr;
$\mathbf{\Omega_j^{Ex}} = (|\Omega_j| - \omega_j^{\max})$: the excess user associated with UAVr;
$\mathbf{\Omega_G}$: the set of users associated with the GBS;
$\mathbf{\Omega_G^{Ex}}$=$(\Omega_G - \omega_G^{\max})$: the excess user associated with GBS;
$D_{\mathbf{j}}^{\mathrm{th}} = \frac{\Omega_j}{\pi * \mathbf{R_j^2}}$: the threshold user density of UAVr;
$\mathbf{R_j}$: the coverage radius of UAVr (36);

Pseudo-code:

Let $\mathrm{P}_j^{\mathrm{Hov}}$ (7) be the required hovering power of each UAVr;
Let the GBS coverage area divide into multiple sub-sectors having radius R_j (36);
Let $\mathbf{P} = \{p_{1,1}, \ldots, p_{i,j}, \ldots, p_{N,K}\}$ be the set of transmission power from the j-th UAVr to the i-th user;
We consider two types of hotspots,
a) density-based, $\omega_j^{\max} = D_j^{\mathrm{th}} * \pi * R_j^2 > 0$,
b) number of user-based, Ω_G^{Ex}=$(\Omega_G - \omega_G^{\max}) > 0$;
for $j = 1$ to K **do**
  while $(\Omega_G^{\mathrm{Ex}} > 0 \vee \Omega_j^{\mathrm{Ex}} > 0) \wedge V_{j \leftarrow s} = 1 \wedge \gamma_{i \leftarrow s} < \gamma_{\mathrm{th}})$ **do**
    Selects the hotspot users i^* from the Ω_G;
    Now CCS sends UAVr U_j^* to serve hotspot users i^*
    */ Start the re-association process, and the transmission power optimization starts */
    for $j = 1$ to K **do**
      for $i = i$ to $|\mathbf{\Omega_j}|$ **do**
        Update $\mathbf{d}_{i^* \leftarrow j^*} = \sqrt{\mathbf{r}_{i^* \leftarrow j^*}^2 + h_j^2}$;
        Determine the average path loss between the selected user and UAVr, $PL^{\mathrm{Avg}}_{h_j^{\mathrm{Ur}}, r_{i^* \leftarrow j^*}}$, by (5) with $\mathbf{d}_{i^* \leftarrow j^*}$;
        Determine the minimum required transmit power $p_{i^* \leftarrow j^*}^{\min}$ for guaranteeing the SINR value (6) of the i-th user by $p_{i^* \leftarrow j^*}^{\min} = \gamma_{\mathrm{th}} \left(B_{i^* \leftarrow j^*} \sigma^2 + I_u\right) / \|\mathbf{h}_{i^* \leftarrow j^*}(t)\|^2$.
        Determine the optimal transmit power $p_{i^* \leftarrow j^*}$ to maximize the E^{Tot} from equation (31) ;
        /* Check the transmit power constraint to make sure $p_{i^* \leftarrow j^*}$ is reasonable, and update $p_{i^* \leftarrow j^*}$. */
        if $p_{i^* \leftarrow j^*}^{\min} \leq p_{\max}$ **then**
          if $p_{i^* \leftarrow j^*} \leq p_{i^*, j^*}^{\min}$ **then**
            $p_{i^* \leftarrow j^*} = p_{i^*, j^*}^{\min}$;
          else if $p_{i^* \leftarrow j^*} \geq p_{\max}$ **then**
            $p_{i^* \leftarrow j^*} = p_{\max}$;
          end if
        else
          $p_{i^* \leftarrow j^*} = p_{\max}$;
        end if
        $\mathbf{P}_{i^* \leftarrow j^*} = p_{i^* \leftarrow j^*}$; // Commit the updated $p_{i^* \leftarrow j^*}$
      end for
    end for
  end while
end for
Check if the hotspot is moving, then deploy UAVr adaptively and maintain the collision distance between the UAVr;
send $\mathbf{\Omega}$, and $\mathbf{P}$ to all UAVr;

Equation (22). Multiple UAVr are dynamically positioned based on user congestion.

- **EGC–SAGIN:** This scheme uses an equal gain combination, where the SINR of the satellite and UAVr links is averaged equally. Multiple UAVr are deployed at the same locations as in AMUD. The only difference from AMUD lies in the SINR combining method.
- **LEO–GBS:** This setup involves only the LEO satellite and GBS. The satellite helps users who cannot be served by GBS when it is visible (Fig. 4) and the SINR condition in Equation (12) is satisfied, and no UAVr are used.
- **GBS–Only:** A purely terrestrial network where users are served only by GBS. Users exceeding the GBS capacity are dropped. Neither satellite assistance nor UAVr is used.

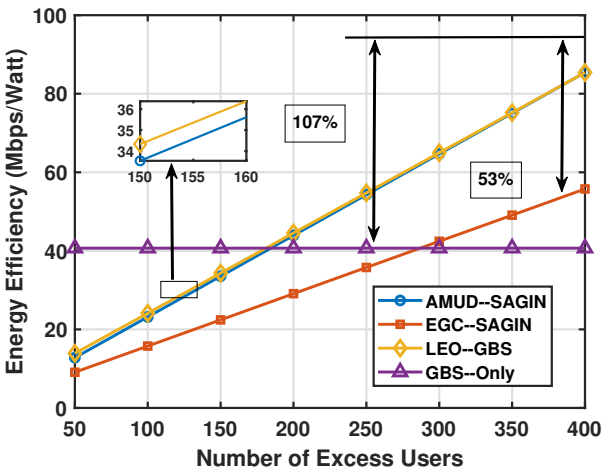

Fig. 6: Performance comparison of the proposed AMUD–SAGIN with other approaches, including EGC–SAGIN, LEO–GBS, and GBS–only, in terms of energy efficiency with varying numbers of excess users.

B. Energy Efficiency Analysis

The simulation evaluates (Fig. 6) the energy efficiency of the proposed AMUD framework in a SAGIN under varying user loads (50:400). When the number of excess users is low, the energy efficiency of AMUD–SAGIN is slightly lower than that of the GBS-only system due to the initial energy overhead of deploying and coordinating multiple UAVr. At lower user loads, this overhead reduces efficiency, as UAVr deployment consumes additional resources even when traffic demand is modest. We also clarify that this overhead is negligible compared to the overall system performance, contributing less than 2% additional signaling load. However, as the user load increases (200–400), AMUD–SAGIN outperforms GBS alone, achieving 107% higher energy efficiency at 400 users. This gain stems from AMUD–SAGIN's dynamic resource allocation and cooperative use of multiple UAVr and LEO satellites to alleviate congestion. Furthermore, AMUD–SAGIN outperforms the EGC–SAGIN scheme by 53%, demonstrating superior adaptability in high-demand environments. Although the energy efficiency curves of AMUD–SAGIN and LEO–GBS appear

visually close, AMUD–SAGIN performs consistently better due to its adaptive link weighting, which prioritizes stronger links and maximizes overall capacity.

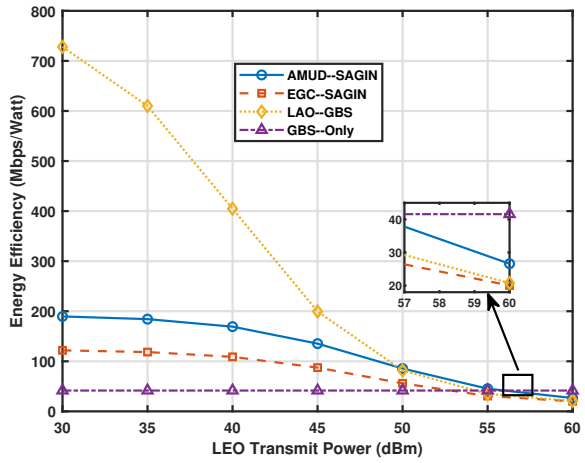

Fig. 7: Performance comparison of the proposed AMUD–SAGIN with other approaches, including EGC–SAGIN, LEO–GBS, and GBS–only, in terms of energy efficiency with varying LEO satellite transmission power levels.

The simulation (Fig. 7) evaluates the energy efficiency of the proposed AMUD–SAGIN framework under varying LEO satellite transmission powers (30–60 dBm) in a SAGIN. When the transmit power of the LEO satellite is low (30 dBm), the energy efficiency of AMUD–SAGIN is slightly lower than that of the LEO–GBS system due to the limited transmission strength of the satellite. However, it still outperforms EGC–SAGIN by 56% and GBS only by 360%, showcasing its ability to leverage UAVr-LEO collaboration even at lower power levels. As the transmit power increases to 60 dBm, AMUD–SAGIN significantly improves its performance, achieving 30% higher energy efficiency than SAGIN and 27% higher than EGC–SAGIN.

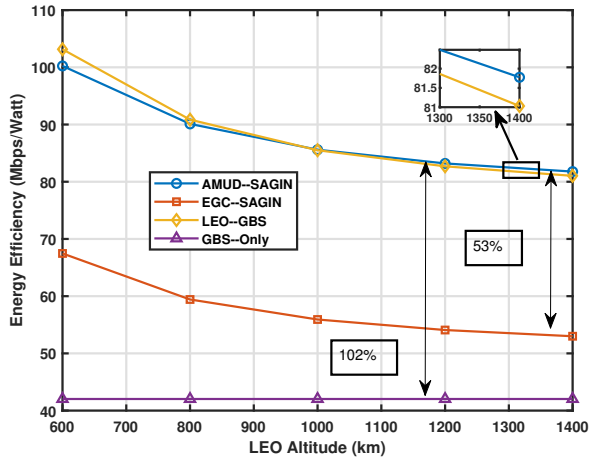

Fig. 8: Performance comparison of the proposed AMUD–SAGIN with other approaches, including EGC–SAGIN, LEO–GBS, and GBS–only, in terms of energy efficiency with varying LEO satellite altitudes.

Fig. 8 illustrates the energy efficiency (Mbps/Watt) as a function of the altitude of the LEO satellite (600–1400 km) with excess users 400. The proposed AMUD–SAGIN approach achieves the highest energy efficiency at 81.74 Mbps/Watt, outperforming LEO–GBS by 2%, EGC–SAGIN by 53% (52.95 Mbps / Watt), and the baseline system only GBS by 102% (41.44 Mbps/Watt). As LEO altitude increases, energy efficiency generally decreases due to higher path loss and increased transmission power requirements. However, AMUD–SAGIN consistently maintains superior performance at varying altitudes, demonstrating its robustness in managing energy consumption through optimized UAVr deployment.

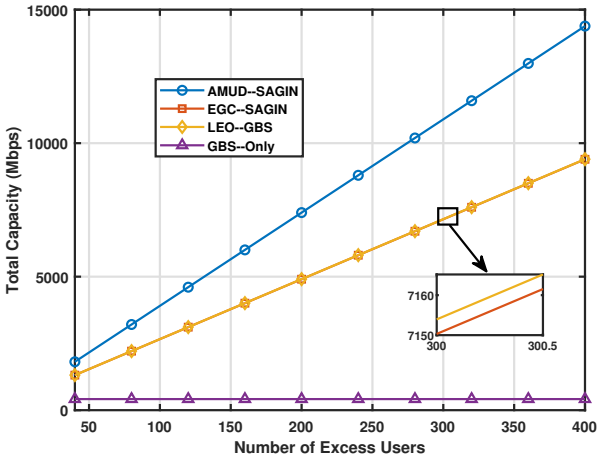

Fig. 9: Performance comparison of the proposed AMUD–SAGIN with other approaches, including EGC–SAGIN, LEO–GBS, and GBS–only, in terms of total capacity with varying excess user counts.

C. *Network Capacity Analysis*

Fig. 9 shows the total capacity (Mbps) as a function of the excess users in various communication schemes (40:400). The proposed AMUD approach consistently outperforms all other schemes, achieving a peak capacity of 14, 386 Mbps for 400 excess users, highlighting its superior scalability and efficiency. In contrast, the LEO-GBS and EGC-SAGIN schemes demonstrate comparable performance, reaching approximately 9, 401 Mbps and 9, 397 Mbps, respectively. This indicates that while both benefit from satellite-ground integration, they lack the dynamic relay deployment capabilities inherent in AMUD–SAGIN. The GBS-only scheme records the lowest capacity, limited to 419 Mbps, due to its dependence solely on terrestrial infrastructure. These findings validate the effectiveness of AMUD-SAGIN in utilizing UAVr to significantly improve network capacity, positioning it as a robust solution for managing high user densities in SAGINs.

D. *The Fairness Analysis*

Fig. 10 illustrates the performance of capacity fairness in different network configurations (10:100). The proposed AMUD framework, along with EGC–SAGIN and LEO–GBS, achieves near-optimal fairness, with fairness indices close to 1.0,

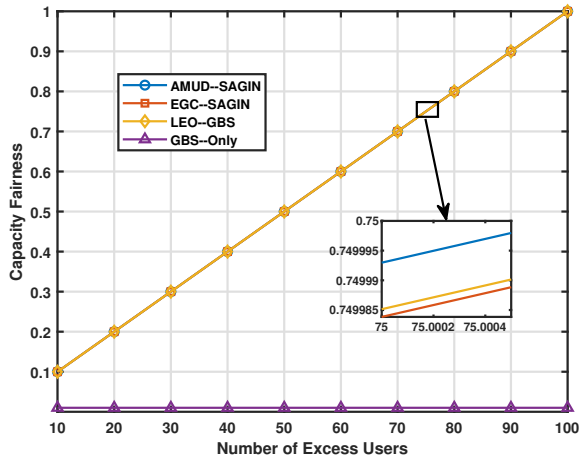

Fig. 10: Performance comparison of the proposed AMUD–SAGIN with other approaches, including EGC–SAGIN, LEO–GBS, and GBS–only, in terms of capacity fairness with varying excess user counts.

indicating an almost uniform distribution of capacity among users. In particular, the fairness levels of AMUD–SAGIN, EGC–SAGIN, and SAGIN are nearly identical, demonstrating their comparable effectiveness in ensuring equitable resource allocation. It is essential to note that simply adding LEO satellite coverage (the baseline LEO-GBS scheme) already addresses the most severe fairness issues by providing a connectivity lifeline to users who would otherwise be dropped by a congested GBS. This explains why all SAGIN-based schemes achieve a near-ideal Jain's fairness index. The primary contribution of the AMUD framework, in this context, is to maintain this high level of fairness while simultaneously optimizing capacity and energy efficiency.

In contrast, the GBS-only configuration performs poorly, with a fairness index of only 0.01, underscoring its inability to distribute capacity fairly among users. This significant disparity underscores the crucial role of UAVrs and satellite integration in ensuring fairness in resource allocation. The results emphasize that while the AMUD–SAGIN, EGC–SAGIN, and LEO–GBS frameworks excel in capacity fairness, the GBS-only network is inadequate in urban areas, reinforcing the need for advanced architectures such as AMUD–SAGIN for equitable and efficient resource management in SAGINs.

VIII. Conclusion

This paper presents the AMUD strategy for integrated satellite air-ground networks. The AMUD framework effectively utilizes multiple UAVr within a LEO satellite-based amplify-and-forward system to enhance the signal-to-interference-plus-noise ratio at the user level. It addresses critical challenges that traditional GBS faces, including increased user density, non-line-of-sight conditions, signal blockages, and difficulty in managing random access users. The AMUD framework emphasizes user fairness in resource allocation while avoiding collisions in multi-UAVr scenarios. In response to dynamic user traffic variations, it adaptively deploys multiple UAVr to maximize user SINR through cooperative diversity-based signal combinations. This is achieved through intelligent communication between LEO satellites, multiple UAVr, and users. The simulation results indicate that the AMUD framework significantly enhances network performance metrics, including total network capacity, energy efficiency, and capacity fairness, particularly under conditions of high user density. These findings underscore the potential of integrating multiple UAVr with LEO satellite technologies to meet the demands of future urban communication networks, especially in scenarios characterized by fluctuating user demands and challenging environmental conditions.

Appendix A
Proof of Signal Combiner

Proof. The weighted combination of the output [49] at the receiver, derived from (1), is expressed as:

$$\gamma_{\mathrm{AF}}(\mathbf{w}) = \text{Signal Power/Noise Power.} \tag{39}$$

The signal power is calculated as:

$$\begin{aligned}\mathbb{E}\left\{\left(\mathbf{w}^{\dagger}\mathbf{h}\right)\mathbf{x}_{\mathrm{sym}}\mathbf{x}_{\mathrm{sym}}^{\dagger}\left(\mathbf{w}\mathbf{h}^{\dagger}\right)\right\} &= \left(\mathbf{w}^{\dagger}\mathbf{h}\right)\mathbb{E}\{\mathbf{x}_{\mathrm{sym}}\mathbf{x}_{\mathrm{sym}}^{\dagger}\}\left(\mathbf{w}\mathbf{h}^{\dagger}\right)\\ &= P_s^{\mathrm{tx}}\left(\mathbf{w}^{\dagger}\mathbf{h}\,\mathbf{w}\,\mathbf{h}^{\dagger}\right)\end{aligned} \tag{40}$$

where $P_s^{\mathrm{tx}} = \mathbb{E}\left\{\mathbf{x}_{\mathrm{sym}}\mathbf{x}_{\mathrm{sym}}^{\dagger}\right\}$. The noise power is calculated as:

$$\mathbb{E}\left\{\left(\mathbf{w}^{\dagger}\mathbf{n}\right)\left(\mathbf{w}^{\dagger}\mathbf{n}\right)^{\dagger}\right\} = \mathbb{E}\left\{\mathbf{w}^{\dagger}\mathbf{n}\mathbf{n}^{\dagger}\mathbf{w}\right\} = \mathbf{w}^{\dagger}\mathbb{E}\left\{\mathbf{n}\mathbf{n}^{\dagger}\right\}\mathbf{w}. \tag{41}$$

Substituting (40) and (41) into (39), we obtain:

$$\gamma_{\mathrm{AF}}(\mathbf{w}) = \frac{P_s^{\mathrm{tx}}\mathbf{w}^{\dagger}\mathbf{h}\mathbf{h}^{\dagger}\mathbf{w}}{\mathbf{w}^{\dagger}\mathbb{E}\left\{\mathbf{n}\mathbf{n}^{\dagger}\right\}\mathbf{w}} = P_s^{\mathrm{tx}}\frac{\mathbf{w}^{\dagger}R_{\mathrm{k}}\mathbf{w}}{\mathbf{w}^{\dagger}\mathscr{R}_{\mathrm{n}}\mathbf{w}}, \tag{42}$$

where $R_{\mathrm{k}} = \mathbf{h}\mathbf{h}^{\dagger}$, and $\mathscr{R}_{\mathrm{n}} = \mathbb{E}\{\mathbf{n}\mathbf{n}^{\dagger}\}$

$$= \mathbb{E}\left\{\begin{bmatrix}\mathbf{n}_{i\leftarrow s}\\ \mathbf{h}_{\mathbf{i}\leftarrow\mathbf{j}\leftarrow\mathbf{s}}\mathcal{G}n_{j\leftarrow s}+\mathbf{n}_{i\leftarrow j\leftarrow s}\end{bmatrix}\begin{bmatrix}\mathbf{n}_{i\leftarrow s}\\ \mathbf{h}_{\mathbf{i}\leftarrow\mathbf{j}\leftarrow\mathbf{s}}\mathcal{G}n_{j\leftarrow s}+\mathbf{n}_{i\leftarrow j\leftarrow s}\end{bmatrix}^{\dagger}\right\}$$

$$= \sigma^2\begin{bmatrix}1 & 0\\ 0 & 1+\mathbf{h}_{i\leftarrow j\leftarrow s}\mathbf{h}_{i\leftarrow j\leftarrow s}^{\dagger}\mathcal{G}^2\end{bmatrix} = \sigma^2\left(\Im_L \oplus R_{\mathrm{M}}\right).$$

□

Appendix B
Proof of Optimal Weight Vector and SINR

Let $u = \mathbf{w}^{\dagger}R_{\mathrm{k}}\mathbf{w}$ and $v = \mathbf{w}^{\dagger}\mathscr{R}_{\mathrm{n}}\mathbf{w}$ from (42), then function $\gamma_{\mathrm{AF}}(\mathbf{w})$ can be write as:

$$\gamma_{\mathrm{AF}}(\mathbf{w}) = u/v \tag{43}$$

Using the quotient rule for derivatives:

$$\frac{d}{d\mathbf{w}}\left(\frac{u}{v}\right) = \frac{v\frac{d}{d\mathbf{w}}(u) - u\frac{d}{d\mathbf{w}}(v)}{v^2}$$

The derivatives of u and v are:

$$d/d\mathbf{w}(u) = 2R_k\mathbf{w}, \quad d/d\mathbf{w}(v) = 2R_n\mathbf{w}$$

Substituting these into the quotient rule:

$$\frac{d}{d\mathbf{w}}\gamma_{\mathrm{AF}}(\mathbf{w}) = \frac{2(\mathbf{w}^{\dagger}R_n\mathbf{w})R_k\mathbf{w} - 2(\mathbf{w}^{\dagger}R_k\mathbf{w})R_n\mathbf{w}}{(\mathbf{w}^{\dagger}R_n\mathbf{w})^2}$$

Setting the derivative to zero leads to:

$$(\mathbf{w}^\dagger R_n \mathbf{w}) R_k \mathbf{w} = (\mathbf{w}^\dagger R_k \mathbf{w}) R_n \mathbf{w}$$

This simplifies to:

$$R_k \mathbf{w} = \lambda R_n \mathbf{w}, \quad \text{where } \lambda = (\mathbf{w}^\dagger R_k \mathbf{w})/(\mathbf{w}^\dagger R_n \mathbf{w})$$

Rewriting: $R_n^{-1} R_k \mathbf{w} = \lambda \mathbf{w}$.

The optimal weight vector $\mathbf{w}_{\text{opt}}$ is the eigenvector of $R_n^{-1} R_k$ corresponding to its largest eigenvalue [45]. Let $\mathbf{h}' = R_n^{-1}\mathbf{h}$. Then:

$$\mathbf{w}_{\text{opt}} = c_r \mathbf{h}' = c_r R_n^{-1} \mathbf{h}, \quad c_r \neq 0$$

Substituting $\mathbf{w}_{\text{opt}}$ into the eigenvalue equation gives:

$$\lambda_{\max} = \mathbf{h}^\dagger R_n^{-1} \mathbf{h}$$

Thus, the optimal weight vector maximizes $\gamma_{\text{AF}}(\mathbf{w})$ and is proportional to $R_n^{-1}\mathbf{h}$.

Step 1: Substitution of $R_n^{-1} = (\mathfrak{I}_L \oplus R_{\text{M}})^{-1}$

$$\frac{p_s^{\text{tx}}}{\sigma^2} \begin{bmatrix} \mathbf{h_{i\leftarrow s}} \\ \mathbf{h_{i\leftarrow j\leftarrow s}} \mathcal{G} \hbar_{j\leftarrow s} \end{bmatrix}^\dagger \left(\mathfrak{I}_L \oplus R_{\text{M}}^{-1}\right) \begin{bmatrix} \mathbf{h_{i\leftarrow s}} \\ \mathbf{h_{i\leftarrow j\leftarrow s}} \mathcal{G} \hbar_{j\leftarrow s} \end{bmatrix}.$$

Step 2: Simplifying the matrix multiplication

The matrix $\left(\mathfrak{I}_L \oplus R_{\text{M}}^{-1}\right)$ acts on the vector $\begin{bmatrix} \mathbf{h_{i\leftarrow s}} \\ \mathbf{h_{i\leftarrow s}} \mathcal{G} \hbar_{j\leftarrow s} \end{bmatrix}$ as:

$$\left(\mathfrak{I}_L \oplus R_{\text{M}}^{-1}\right) \begin{bmatrix} \mathbf{h_{i\leftarrow s}} \\ \mathbf{h_{i\leftarrow s}} \mathcal{G} \hbar_{j\leftarrow s} \end{bmatrix} = \begin{bmatrix} \mathbf{h_{i\leftarrow s}} \\ R_{\text{M}}^{-1} \cdot \mathbf{h_{i\leftarrow s}} \mathcal{G} \hbar_{j\leftarrow s} \end{bmatrix}.$$

This yields the following.

$$\frac{p_s^{\text{tx}}}{\sigma^2} \begin{bmatrix} \mathbf{h_{i\leftarrow s}} \\ \mathbf{h_{i\leftarrow s}} \mathcal{G} \hbar_{j\leftarrow s} \end{bmatrix}^\dagger \begin{bmatrix} \mathbf{h_{i\leftarrow s}} \\ R_{\text{M}}^{-1} \cdot \mathbf{h_{i\leftarrow s}} \mathcal{G} \hbar_{j\leftarrow s} \end{bmatrix}.$$

Step 3: Expanding the inner product:

$$\frac{p_s^{\text{tx}}}{\sigma^2} \left(\mathbf{h_{i\leftarrow s}}^\dagger \mathbf{h_{i\leftarrow s}} + \left(\mathbf{h_{i\leftarrow s}} \mathcal{G} \hbar_{j\leftarrow s}\right)^\dagger R_{\text{M}}^{-1} \cdot \left(\mathbf{h_{i\leftarrow s}} \mathcal{G} \hbar_{j\leftarrow s}\right) \right).$$

The first term is simply $|\mathbf{h_{i\leftarrow s}}|^2$, and the given: $R_{\text{M}} = 1 + \mathbf{h_{i\leftarrow s}} \mathbf{h_{i\leftarrow s}}^\dagger \mathcal{G}^2$, and substituting this into the second term:

$$\begin{aligned} &= \frac{p_s^{\text{tx}}}{\sigma^2} \left(|\mathbf{h}_{i\leftarrow s}|^2 + \frac{\left|\mathbf{h}_{i\leftarrow j\leftarrow s} \mathcal{G}\right|^2 \left|\hbar_{j\leftarrow s}\right|^2}{1 + \left|\mathbf{h}_{i\leftarrow j\leftarrow s} \mathcal{G}\right|^2} \right) \\ &= \gamma_{i\leftarrow s} + \gamma_{i\leftarrow j} (\left\|\hbar_{j\leftarrow s}\right\|^2)/(1 + \left\|\mathbf{h}_{i\leftarrow j\leftarrow s} \mathcal{G}\right\|^2) \end{aligned}$$

Multiply $\frac{p_s^{\text{tx}}}{\sigma^2}$ into the expression:

$$= \gamma_{i\leftarrow s} + \gamma_{i\leftarrow j} \frac{\frac{p_s^{\text{tx}}}{\sigma^2} \left\|\hbar_{j\leftarrow s}\right\|^2}{\frac{p_s^{\text{tx}}}{\sigma^2} \left(1 + \left\|\mathbf{h}_{i\leftarrow j\leftarrow s} \mathcal{G}\right\|^2\right)} = \gamma_{i\leftarrow s} + \frac{\gamma_{i\leftarrow j} \gamma_{j\leftarrow s}}{\gamma_{i\leftarrow j} + \varsigma}. \tag{44}$$

where $\varsigma = \frac{1}{\sigma^2 \mathcal{G}^2}$ [50], $R_{\text{M}} = \mathfrak{I}_L + \mathcal{G}^2 \mathbf{h_{i\leftarrow j\leftarrow s}} \mathbf{h_{i\leftarrow j\leftarrow s}}^\dagger$ represents the covariance matrix of $\mathbf{n}$, $\mathfrak{I}_L$ is the identity matrix $L * L$.

REFERENCES

[1] Bhola, Y.-J. Chen, A. Balakrishnan, S. De, and L.-C. Wang, "Cooperative UAV-Relay based satellite aerial ground integrated networks," in *2024 IEEE 100th Vehicular Technology Conference (VTC2024-Fall)*, 2024, pp. 1–5.

[2] Y. Liu, S. Zhang, X. Mu, Z. Ding, R. Schober, N. Al-Dhahir, E. Hossain, and X. Shen, "Evolution of NOMA toward next-generation multiple access (NGMA) for 6G," *IEEE J. Sel. Areas Commun.*, vol. 40, no. 4, pp. 1037–1071, 2022.

[3] Y. Aydin, G. K. Kurt, E. Ozdemir, and H. Yanikomeroglu, "Group handover for drone base stations," *IEEE IoT J.*, vol. 8, no. 18, pp. 13 876–13 887, 2021.

[4] A. Guidotti, A. Vanelli-Coralli, M. Conti, S. Andrenacci, S. Chatzinotas, N. Maturo, B. Evans, A. Awoseyila, A. Ugolini, T. Foggi, L. Gaudio, N. Alagha, and S. Cioni, "Architectures and key technical challenges for 5G systems incorporating satellites," *IEEE Trans. Veh. Technol.*, vol. 68, no. 3, pp. 2624–2639, 2019.

[5] M. Giordani and M. Zorzi, "Non-terrestrial networks in the 6G era: Challenges and opportunities," *IEEE Netw.*, vol. 35, no. 2, pp. 244–251, 2021.

[6] A. Balakrishnan, S. De, and L.-C. Wang, "Haps-aided power grid connected green communication framework: Architecture and optimization," in *ICC 2024-IEEE International Conference on Communications*. IEEE, 2024, pp. 2847–2852.

[7] Y.-J. Chen, W. Chen, and M.-L. Ku, "Trajectory design and link selection in UAV-assisted hybrid satellite-terrestrial network," *IEEE Commun. Lett.*, vol. 26, no. 7, pp. 1643–1647, 2022.

[8] H. Al-Hraishawi, H. Chougrani, S. Kisseleff, E. Lagunas, and S. Chatzinotas, "A survey on nongeostationary satellite systems: The communication perspective," *Commun. Surveys Tuts.*, vol. 25, no. 1, p. 101–132, 2023.

[9] A. Balakrishnan, P. Popineau, and P. Martins, "Timing advance and doppler shift estimation in leo satellite networks: A recursive bayesian study," *arXiv preprint arXiv:2506.08739*, 2025.

[10] *3GPP Technical Specification Group Services and System Aspects; Unmanned aerial system (UAS) support in 3GPP*, 3GPP Standard TS 22.125 V17.2.0, October, 2020.

[11] P. K. Sharma, D. Deepthi, and D. I. Kim, "Outage probability of 3-D mobile UAV relaying for hybrid satellite-terrestrial networks," *IEEE Commun. Lett.*, vol. 24, no. 2, pp. 418–422, 2020.

[12] Y. Zhao, H. Chen, L. Xie, and K. Wang, "Exact and asymptotic ergodic capacity analysis of the hybrid satellite-terrestrial cooperative system over generalized fading channels," *IET Communications*, vol. 12, no. 11, pp. 1342–1350, 2018.

[13] R. Dubey, A. Balakrishnan, and S. De, "Intelligent uav swarm coexistence in dtv bands," in *2024 IEEE 100th Vehicular Technology Conference (VTC2024-Fall)*. IEEE, 2024, pp. 1–5.

[14] C.-C. Lai, Bhola, A.-H. Tsai, and L.-C. Wang, "Adaptive and fair deployment approach to balance offload traffic in multi-UAV cellular networks," *IEEE Trans. Veh. Technol.*, vol. 72, no. 3, pp. 3724–3738, 2023.

[15] P. K. Singya and M.-S. Alouini, "Performance of UAV-assisted multiuser terrestrial-satellite communication system over mixed FSO/RF channels," *IEEE Transactions on Aerospace and Electronic Systems*, vol. 58, no. 2, pp. 781–796, 2022.

[16] A. Hajijamali Arani, M. M. Azari, P. Hu, Y. Zhu, H. Yanikomeroglu, and S. Safavi-Naeini, "Reinforcement learning for energy-efficient trajectory design of UAVs," *IEEE IoT J.*, vol. 9, no. 11, pp. 9060–9070, 2022.

[17] Bhola, C.-C. Lai, and L.-C. Wang, "The outage-free replacement problem in unmanned aerial vehicle base stations," *IEEE Transactions on Vehicular Technology*, vol. 70, no. 12, pp. 13 390–13 395, 2021.

[18] V. Singh, P. K. Upadhyay, and M. Lin, "On the performance of NOMA-assisted overlay multiuser cognitive satellite-terrestrial networks," *IEEE Wireless Commun. Lett.*, vol. 9, no. 5, pp. 638–642, 2020.

[19] Q. Huang, M. Lin, W.-P. Zhu, S. Chatzinotas, and M.-S. Alouini, "Performance analysis of integrated satellite-terrestrial multiantenna relay networks with multiuser scheduling," *IEEE Transactions on Aerospace and Electronic Systems*, vol. 56, no. 4, pp. 2718–2731, 2020.

[20] S. Sreng, B. Escrig, and M.-L. Boucheret, "Exact symbol error probability of Hybrid/Integrated satellite-terrestrial cooperative network," *IEEE Trans. Wireless Commun.*, vol. 12, no. 3, pp. 1310–1319, 2013.

[21] Z. Zhao, G. Xu, N. Zhang, and Q. Zhang, "Performance analysis of the hybrid satellite-terrestrial relay network with opportunistic scheduling over generalized fading channels," *IEEE Transactions on Vehicular Technology*, vol. 71, no. 3, pp. 2914–2924, 2022.

[22] T. Qi, W. Feng, and Y. Wang, "Outage performance of non-orthogonal multiple access based unmanned aerial vehicles satellite networks," *China Communications*, vol. 15, no. 5, pp. 1–8, 2018.

[23] N. Wang, F. Li, D. Chen, L. Liu, and Z. Bao, "NOMA-based energy-efficiency optimization for UAV enabled space-air-ground integrated relay networks," *IEEE Transactions on Vehicular Technology*, vol. 71, no. 4, pp. 4129–4141, 2022.

[24] T. Akiyoshi, E. Okamoto, H. Tsuji, and A. Miura, "Performance improvement of satellite/terrestrial integrated mobile communication system using unmanned aerial vehicle cooperative communications," in *2017 International Conference on Information Networking (ICOIN)*, 2017, pp. 417–422.

[25] H. Kong, M. Lin, W.-P. Zhu, H. Amindavar, and M.-S. Alouini, "Multiuser scheduling for asymmetric FSO/RF links in satellite-UAV-terrestrial networks," *IEEE Wireless Commun. Lett.*, vol. 9, no. 8, pp. 1235–1239, 2020.

[26] A. Ranjha and G. Kaddoum, "URLLC facilitated by mobile UAV relay and RIS: A joint design of passive beamforming, blocklength, and UAV positioning," *IEEE Internet of Things Journal*, vol. 8, no. 6, pp. 4618–4627, 2021.

[27] Z. Kang, C. You, and R. Zhang, "Placement learning for multi-UAV relaying: A Gibbs sampling approach," in *ICC 2020 - 2020 IEEE International Conference on Communications (ICC)*, 2020, pp. 1–6.

[28] D. Qin, Y. Wang, F. Zhou, and K.-K. Wong, "Performance analysis of AF relaying with selection combining in nakagami-m fading," *IEEE Sys. J.*, vol. 13, no. 3, pp. 2375–2385, 2019.

[29] P. Som and A. Chockalingam, "Bit error probability analysis of SSK in DF relaying with threshold-based best relay selection and selection combining," *IEEE Commun. Lett.*, vol. 18, no. 1, pp. 18–21, 2014.

[30] X. Fang, W. Feng, T. Wei, Y. Chen, N. Ge, and C.-X. Wang, "5G embraces satellites for 6G ubiquitous IoT: Basic models for integrated satellite terrestrial networks," *IEEE IoT J.*, vol. 8, no. 18, pp. 14 399–14 417, 2021.

[31] L. Sanguinetti, A. A. D'Amico, and Y. Rong, "A tutorial on the optimization of Amplify-and-Forward MIMO Relay systems," *IEEE Journal on Selected Areas in Communications*, vol. 30, no. 8, pp. 1331–1346, 2012.

[32] A. Al-Hourani, S. Kandeepan, and S. Lardner, "Optimal LAP altitude for maximum coverage," *IEEE Wireless Commun. Lett.*, vol. 3, no. 6, pp. 569–572, 2014.

[33] A. Al-Hourani, S. Kandeepan, and A. Jamalipour, "Modeling air-to-ground path loss for low altitude platforms in urban environments," in *IEEE GLOBECOM*, 2014, pp. 2898–2904.

[34] M.-H. T. Nguyen, T. T. Bui, L. D. Nguyen, E. Garcia-Palacios, H.-J. Zepernick, H. Shin, and T. Q. Duong, "Real-time optimized clustering and caching for 6G satellite-UAV-terrestrial networks," *IEEE Transactions on Intelligent Transportation Systems*, pp. 1–11, 2023.

[35] J. Wang, C. Jiang, Z. Wei, C. Pan, H. Zhang, and Y. Ren, "Joint UAV hovering altitude and power control for space-air-ground IoT networks," *IEEE IoT J.*, vol. 6, no. 2, pp. 1741–1753, 2019.

[36] X. Lin, S. Cioni, G. Charbit, N. Chuberre, S. Hellsten, and J.-F. Boutillon, "On the path to 6G: Embracing the next wave of low earth orbit satellite access," *IEEE Communications Magazine*, vol. 59, no. 12, pp. 36–42, 2021.

[37] P. Zong and S. Kohani, "Optimal satellite LEO constellation design based on global coverage in one revisit time," *International Journal of Aerospace Engineering*, vol. 2019, pp. 1–12, 2019.

[38] W. Abderrahim, O. Amin, M.-S. Alouini, and B. Shihada, "Proactive traffic offloading in dynamic integrated multi-satellite terrestrial networks," *IEEE Trans. Commun.*, vol. 70, no. 7, pp. 4671–4686, 2022.

[39] A. Omran, M. Cheriet, and L. Sboui, "UAV-assisted offloading via satellite backhaul for post-disaster and crowded cellular networks," in *2023 IEEE Globecom Workshops (GC Wkshps)*, 2023, pp. 824–829.

[40] P. K. Chowdhury, M. Atiquzzaman, and W. Ivancic, "Handover schemes in satellite networks: state-of-the-art and future research directions," *IEEE Commun. Surv. Tutor.*, vol. 8, no. 4, pp. 2–14, 2006.

[41] M. Alzenad, A. El-Keyi, F. Lagum, and H. Yanikomeroglu, "3-D placement of an unmanned aerial vehicle base station (UAV-BS) for energy-efficient maximal coverage," *IEEE Wireless Commun. Lett.*, vol. 6, no. 4, pp. 434–437, 2017.

[42] Y. Labrador, M. Karimi, D. Pan, and J. Miller, "An approach to cooperative satellite communications in 4G mobile systems." *J. Commun.*, vol. 4, no. 10, pp. 815–826, 2009.

[43] Y.-W. P. Hong, W.-J. Huang, and C.-C. J. Kuo, *Cooperative communications and networking: technologies and system design*. Springer Science & Business Media, 2010.

[44] Z. Zhang, Y. Li, C. Huang, Q. Guo, L. Liu, C. Yuen, and Y. L. Guan, "User activity detection and channel estimation for grant-free random access in LEO satellite-enabled internet of things," *IEEE Internet of Things Journal*, vol. 7, no. 9, pp. 8811–8825, 2020.

[45] B. Holter and G. E. Oien, "The optimal weights of a maximum ratio combiner using an eigenfilter approach," in *5th Nordic Signal Processing Symposium*. Citeseer, 2002.

[46] R. K. Jain, D.-M. W. Chiu, W. R. Hawe *et al.*, "A quantitative measure of fairness and discrimination," *Eastern Research Laboratory, Digital Equipment Corporation, Hudson, MA*, vol. 21, 1984.

[47] R. Sun, M. Hong, and Z.-Q. Luo, "Joint downlink base station association and power control for max-min fairness: Computation and complexity," *IEEE Journal on Selected Areas in Communications*, vol. 33, no. 6, pp. 1040–1054, 2015.

[48] Drone laws in Taiwan. Access on July. 8, 2022. [Online]. Available: https: //uavcoach.com/drone-laws-in-taiwan/

[49] A. K. Jagannatham, *Principles of modern wireless communication systems*. McGraw-Hill Education, 2015.

[50] O. S. Badarneh and M. Kadoch, "Performance analysis of dual-hop systems with fixed-gain relays over generalized η-μ fading channels," in *2012 IEEE Global Communications Conference (GLOBECOM)*, 2012, pp. 4148–4152.